Nordic Seas Acidification

Filippa Fransner[1], Friederike Fröb[2], Jerry Tjiputra[3], Melissa Chierici[4], Agneta Fransson[5], Nadine Goris[3], Emil Jeansson[3], Truls Johannessen[1], Elizabeth Jones[4], Siv K. Lauvset[3], Sólveig R. Ólafsdóttir[6], Abdirahman Omar[3], Ingunn Skjelvan[3], and Are Olsen[1]

[1]Geophysical Institute, University of Bergen, and Bjerknes Centre for Climate Research, Bergen, Norway
[2]Max Planck Institute for Meteorology, Hamburg, Germany
[3]NORCE Norwegian Research Centre, Bjerknes Centre for Climate Research, Bergen, Norway
[4]Institute of Marine Research, Fram Centre, Tromsø, Norway
[5] Norwegian Polar Institute, Tromsø, Norway
[6]Marine and Freshwater Research Institute, Reykjavík, Iceland

Correspondence: Filippa Fransner (filippa.fransner@uib.no)

Abstract.

With prevailing low temperatures, deep winter mixing, and cold-water coral reefs, the Nordic Seas is vulnerable to ocean acidification. Here we present a detailed investigation of changes in pH and aragonite saturation, and its impact on cold-water corals, in the Nordic Seas, from pre-industrial times to 2100 by using *in situ* observations, gridded climatological data, and Earth System Model (ESM) projections. From pre-industrial to present, the Nordic Seas surface pH has dropped by 0.06 on average, and the aragonite saturation horizon has moved from a depth of 2500 meter to 2000m, which is well below the cold-water coral habitats. Between 1981 and 2019 pH decreased by, on average, 0.10 in the Nordic Seas surface waters. The pH drop, mainly driven by an uptake of anthropogenic CO_2, is significant all over the Nordic Seas, except in the Barents Sea Opening. We also find that the acidification has penetrated relatively deep, in some regions down to 2000 m. This has resulted in a significant decrease in the aragonite saturation state, which are close to undersaturation in the depth layer of 1000-2000 m in the modern ocean. Model projections indicate an additional surface ocean pH decrease of 0.1-0.4 until the year of 2100. In the high-emission scenario, RCP8.5, the entire water column is projected to be undersaturated in aragonite by the end of the century, threatening Nordic Seas' cold-water corals and their ecosystems. Under the emission-driven RCP4.5 scenario the saturation horizon is projected to be lifted to 400-800 m by the end of this century, endangering the deepest living cold-water corals. Exposure of cold-water corals to corrosive waters can only be avoided under the emission-driven RCP2.6 scenario. Over all time scales, the main driver of the pH drop is an increase in dissolved inorganic carbon, which to some extent is opposed by increasing alkalinity. Temperature and salinity effects are of secondary importance.

1 Introduction

Since 1850, human activities have released 650 $\pm$ 65 Gt of carbon to the atmosphere, of which about 25% have been taken up by the oceans (Friedlingstein et al., 2020) where it has added to the pool of dissolved inorganic carbon (C_T). The increasing C_T has resulted in surface seawater pH decline of approximately 0.1, which corresponds to an approximately 30% increase in hydrogen ion (H^+) concentration (e.g., Doney et al., 2009; Gattuso and Hansson, 2011; Jiang et al., 2019). This ocean acidification is a serious threat to many marine organisms, in particular those having shells and skeletons consisting of calcium carbonate ($CaCO_3$), such as pteropods and corals (Guinotte et al., 2006; Turley et al., 2007; Manno et al., 2017; Doney et al., 2020; Doo et al., 2020) as the pH drop also leads to a reduction in the $CaCO_3$ saturation state (Ω) of seawater. Depending on the CO_2 concentration pathway, future projections suggest further reductions of surface ocean pH of 0.1-0.4 until the end of the 21st century from the 1990s (Bopp et al., 2013). While global average acidification rates for surface waters, both from pre-industrial times to present and as projected for the future have been dealt with in several studies (e.g. Caldeira and Wickett, 2003; Raven et al., 2005; Kwiatkowski et al., 2020), less is known about acidification rates on regional scales, especially below the surface.

The Nordic Seas, comprised of the Greenland, Iceland and Norwegian seas (Fig. 1) and bounded by the Fram Strait in the north, the Barents Sea Opening to the northeast and the Greenland-Scotland Ridge in the south, are of particular interest when it comes to ocean acidification due to its specific dynamic, biogeochemical and ecosystem characteristics. The surface circulation pattern (e.g. Blindheim and Østerhus, 2013; Våge et al., 2013) is characterised by the warm, saline Atlantic waters that flow northward as the Norwegian Atlantic Current in the east, mainly constrained to the Norwegian Sea, and cold and fresh waters of Arctic origin flowing southward as the East Greenland Current in the west. The surface waters are undersaturated in pCO_2, i.e. their pCO_2 is lower than that of the atmosphere, making them important sinks for atmospheric CO_2. This undersaturation comes as a result of several processes, including strong primary production, cooling of northward flowing Atlantic waters, and the inflow of pCO_2 undersaturated waters from the Arctic Ocean (Olsen et al., 2008; Ólafsson et al., 2020b). In the Greenland and Iceland seas, deep and intermediate water-masses are formed through open-ocean convection. Some of these water-masses ultimately overflow the Greenland-Scotland Ridge and feed into the North Atlantic Deep Water and consequently help to sustain the lower limb of the Atlantic Meridional Overturning Circulation (AMOC, Dickson and Brown, 1994; Våge et al., 2015; Chafik and Rossby, 2019). The strong connection between surface and deep waters that is created through this deep water formation, would ultimately lead to early and relatively large detection of anthropogenic carbon and acidification in the deep waters of the Nordic Seas and North Atlantic (Tjiputra et al., 2010; Perez et al., 2018), which could have negative impacts on their cold-water coral reefs. Due to the prevailing low temperatures, the Nordic Seas already have naturally low saturation states of $CaCO_3$ (Ólafsson et al., 2009; Skjelvan et al., 2014), making their cold-water coral reefs particularly exposed to ocean acidification (Kutti et al., 2014).

There has been extensive research on changes in the carbonate system and pH in the Nordic Seas, facilitated by the many research and monitoring cruises in the area (e.g., Bellerby et al., 2005; Olsen et al., 2006; Ólafsson et al., 2009; Skjelvan et al., 2008; Chierici et al., 2012; Skjelvan et al., 2014; Jones et al., 2020; Skjelvan et al., 2021). Acidification rates of -0.0023 to

-0.0041 y^{-1} have been observed in surface waters, which is greater than expected from the increase in atmospheric CO_2 alone (Ólafsson et al., 2009; Skjelvan et al., 2014). This is consistent with the many observations that have indicated that surface ocean pCO_2, which is closely related to pH, has risen faster than the atmospheric pCO_2 (Olsen et al., 2006; Skjelvan et al., 2008; Ólafsson et al., 2009), i.e. a weakening of the pCO_2 undersaturation of the Nordic Seas surface waters might have occurred the past decades. Studies on present and future pH in the Nordic Seas using both a regional and an Earth System Model have also been published (Skogen et al., 2014, 2018). There is, however, to our knowledge, no previous work assessing acidification rates from the pre-industrial until the end of the 21st century using both observational and modelling data.

In this study, we fill this gap by examining past, present and projected future ocean acidification rates and changes in aragonite saturation in the Nordic Seas, over the full water column, by using the best available information for the various time periods. This includes a combination of *in situ* observations, gridded climatological data, and Earth System Model (ESM) projections. To get a better understanding of the processes behind the acidification rates, we decompose the pH changes into their thermodynamic and chemical drivers.

1.1 pH Drivers - Theoretical Background

The rising atmospheric CO_2 concentration increases the pCO_2 difference between the atmosphere and the ocean; i.e. the oceans become more undersaturated in CO_2 with respect to the atmosphere, which results in a flux of CO_2 from the atmosphere into the ocean. When CO_2 dissolves in seawater, it reacts with water to form carbonic acid (H_2CO_3):

$$CO_2 + H_2O \rightleftharpoons H_2CO_3 \tag{1}$$

which then dissociates into bicarbonate (HCO_3^-) and hydrogen ions (H^+):

$$H_2CO_3 \rightleftharpoons HCO_3^- + H^+ \tag{2}$$

A large part of the resulting H^+ is neutralized by carbonate ions (CO_3^{2-}) that have been supplied to the ocean by the weathering of carbonate and silicious minerals:

$$CO_3^{-2} + H^+ \rightleftharpoons HCO_3^- \tag{3}$$

Combined, the concentration of CO_2 ($CO_{2(aq)}$), H_2CO_3, HCO_3^-, and CO_3^{2-}, constitute the concentration of dissolved inorganic carbon (C_T), while total alkalinity (A_T) is mostly determined by HCO_3^-, and CO_3^{2-} (carbonate alkalinity). In seawater, approximately 90% of C_T exists in the form of HCO_3^-, 9% as CO_3^{2-} and 1% as $CO_{2(aq)}$.

As seen from Equations 1 - 3, the dissolution of CO_2 in seawater results in an increase in H^+ concentration, which leads to a decrease in pH, defined as:

$$pH = -log_{10}([H^+]) \tag{4}$$

Apart from C_T, seawater pH is also controlled by temperature, salinity, and A_T. The qualitative, instantaneous, effects of an increase in each property are shown in Table 1. Temperature and salinity only affect pH by altering the dissociation constants and thus the partitioning of C_T between its different constituents. A_T is the sum of the concentration of bases (proton acceptors) in the seawater. The relation between C_T and A_T influences the pH by affecting the buffer capacity of seawater. Note that the relations in Table 1 are the instantaneous, or thermodynamic, effects from a change in these properties, and does not consider indirect effects on pH, for example from the change in air-sea fluxes that will follow, e.g. from a temperature driven pCO_2 change (e.g. Jiang et al., 2019; Wu et al., 2019).

Table 1. Direction of instantaneous effects of an increase in temperature, salinity, C_T and A_T on pH and Ω.

Driver	pH	Ω
Temperature	-	+
Salinity	-	-
C_T	-	-
A_T	+	+

Equations 2 and 3 can be summarized as:

$$H_2CO_3 + CO_3^{2-} \longrightarrow 2HCO_3^- \tag{5}$$

showing that the dissolution of CO_2 in seawater results in a reduction in CO_3^{2-}. This further affects the saturation state of $CaCO_3$ (Ω), defined as:

$$\Omega = \frac{[Ca^{2+}][CO_3^{2-}]}{K_{sp}} \tag{6}$$

where K_{sp} is the solubility product. $CaCO_3$ exists in two different forms in seawater: calcite and aragonite. Aragonite is more soluble than calcite, with a higher K_{sp}. The saturation state of aragonite (Ω_{Ar}) is therefore lower than that of calcite (Ω_{Ca}) at a given place and time. When Ω is less than one, the water is corrosive and $CaCO_3$ dissolves.

Equation 6 shows that lower concentrations of CO_3^{2-}, as induced by uptake of anthropogenic CO_2 and increase in C_T, result in a reduction in the saturation state. The impact of C_T on the saturation state is also seen in the spatial distribution of Ω in the surface ocean, which broadly follows temperature gradients (e.g. Orr, 2011; Jiang et al., 2019). The reason behind this temperature dependency is the higher CO_2 solubility of colder waters that give them the capacity to absorb more CO_2 at a given atmospheric pCO_2, which decreases the CO_3^{2-} concentration. Consequently, cold waters also have a relatively low Ω_{Ar} and Ω_{Ca} and are thus more vulnerable to acidification. Apart from C_T, Ω is also influenced by A_T, temperature and salinity, as shown in Table 1.

The sensitivity of pH and Ω to uptake of anthropogenic CO_2 is dependent on the buffer capacity of the seawater that is largely determined by the concentration of carbonate ions [CO_3^{2-}] (e.g. Sarmiento and Gruber, 2006; Orr, 2011). Waters with

higher concentrations of CO_3^{2-}, i.e. a higher buffer capacity, have the capability of converting a larger fraction of the absorbed CO_2 into bicarbonate. A smaller fraction remains as dissolved CO_2, implying a smaller increase in the seawater pCO_2. These waters therefore have the capability of absorbing more CO_2 for any given increase in atmospheric pCO_2 (assuming a uniform increase in pCO_2 between water-masses), which also implies a larger decline in $CaCO_3$ saturation state. The drop in pH, on the other hand, is larger in waters with lower CO_3^{2-} concentration as they have less ability to neutralise the carbonic acid since their buffer capacity is lower.

2 Data and methods

2.1 Data

2.1.1 Observational data

This study makes use of C_T, A_T, temperature, salinity, phosphate and silicate data collected between 1981 and 2019 during dedicated research cruises, at two time-series stations, and in the framework of the program "Monitoring ocean acidification in Norwegian waters". Sampling locations are shown in Fig. 1.

Data from 28 research cruises (Brewer et al., 2010; Anderson et al., 2013a, b; Anderson, 2013a, b; Bellerby and Smethie, 2013; Johannessen and Golmen, 2013; Johannessen, 2013a, b; Johannessen and Simonsen, 2013; Johannessen and Olsen, 2013; Johannessen et al., 2013c, a, b; Jones et al., 2013; Olsen et al., 2013; Olsen and Omar, 2013; Omar and Olsen, 2013; Omar and Skogseth, 2013; Omar, 2013; Pegler et al., 2013; Skjelvan et al., 2013; Wallace and Deming, 2014; Lauvset et al., 2016; Tanhua, 2017; Jeansson et al., 2018; Marcussen, 2018; Schauer et al., 2018) in the Nordic Seas were extracted from the GLODAPv2.2019 data product, which provides bias-corrected, cruise based, interior ocean data (Olsen et al., 2019). The GLODAPv2 data product is considered consistent to within 0.005 for salinity, 2% for silicate , 2% for phosphate, 4 μmol kg^{-1} for C_T and 4 μmol kg^{-1} for A_T (Olsen et al., 2019).

The time-series data are from the Norwegian Sea (Ocean Weather Station M) and the Iceland Sea. The data from the Ocean Weather Station M, located at 66 °N and 2 °E, have been described in Skjelvan et al. (2008). At this station, sampling at 12 depth levels between surface and seabed (2100 m) was carried out each month between 2002 and 2009, and 4-6 times each year between 2010 and 2019. Here, the uncertainty related to the sample data is 0.001 for salinity, 0.7 μmol kg^{-1} for silicate , 0.06 μmol kg^{-1} for phosphate, 2 μmol kg^{-1} for C_T and 2 μmol kg^{-1} for A_T. The time-series station in the Iceland Sea, covering the period of 1985-2019, is situated at 68 °N and 12.67 °W. It is visited approximately 4 times a year and samples are taken at 10-20 depth levels between surface and seabed (1900 m). The uncertainty related to the sampled data at this station is 0.005 for salinity, 2% for silicate , 2% for phosphate, 4 μmol kg^{-1} for C_T and 4 μmol kg^{-1} for A_T. These data have been described in Ólafsson et al. (2009).

The data from the program" Monitoring ocean acidification in Norwegian waters" covers the period 2011-2019 (2011-2012 Tilførselsprogrammet and 2013-2019 Havforsuringsprogrammet) and are based on water column stations along repeat sections in the Nordic Seas (Chierici et al., 2012, 2013, 2014, 2015, 2016, 2017; Jones et al., 2018, 2019, 2020). Analytical methods for

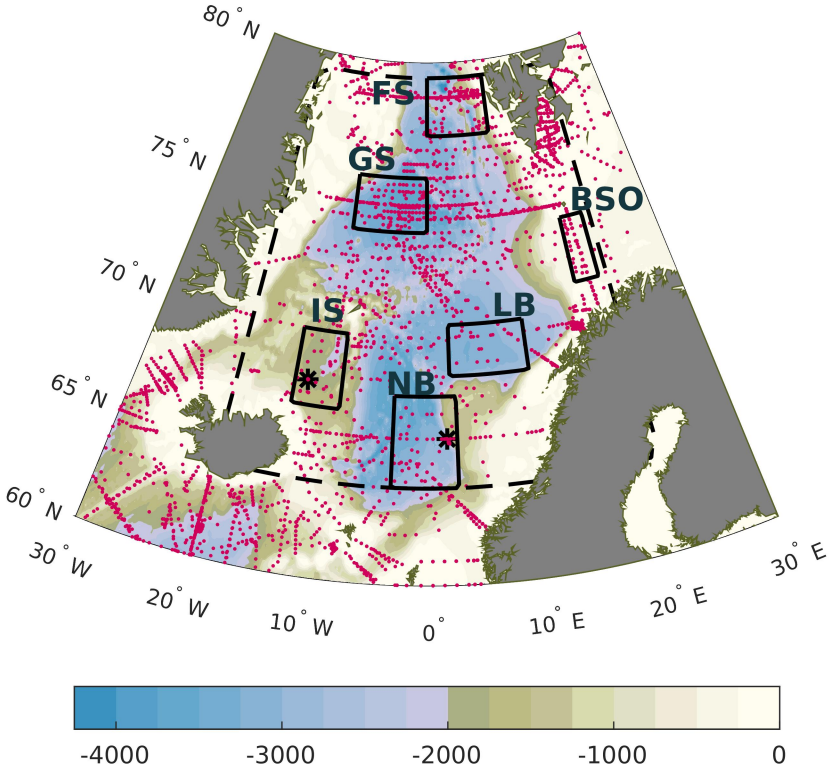

Figure 1. Map of the Nordic Seas with sampling locations (magenta). Also shown are the locations of the six regions where trends have been analyzed (rectangles); BSO: Barents Sea Opening; FS: Eastern Fram Strait; GS: Greenland Sea; IS: Iceland Sea; LB: Lofoten Basin; NB: Norwegian Basin. The dashed line marks the area that we define as the Nordic Seas. The asterisk markers in the Norwegian Basin and the Iceland Sea show the positions of Ocean Weather station M and the Iceland Sea time-series station, respectively. The filled contours illustrate the bathymetry at 250 m intervals.

C_T and A_T follow the Dickson et al. (2007) and accuracy and precision is controlled by Certified Reference Materials (CRM), and by participation in international intercomparison studies (e.g. Bockmon and Dickson, 2015). The uncertainties related to the sampled data is 0.005 for salinity, 0.1 for silicate , 0.06 for phosphate, 2 μmol kg^{-1} for C_T and 2 μmol kg^{-1} for A_T.

Data for the Eastern Fram Strait were collected on cruises with RV Helmer Hansen within the CarbonBridge project, and on cruises with RV Lance (Chierici et al., 2019b) organized by the Norwegian Polar Institute.

For atmospheric CO_2 data, we used the annual mean atmospheric CO_2 mole fraction (xCO_2) from the Mauna Loa updated records, downloaded from www.esrl.noaa.gov/gmd/ccgg/trends/ .

2.1.2 Model data

For the estimates of past and future ocean acidification under various climate scenarios, we used output of the fully coupled Norwegian Earth System Model (NorESM1-ME, Bentsen et al., 2013; Tjiputra et al., 2013, 2016) as well as outputs of an ensemble of ESMs that participated in the Coupled Model Intercomparison Project Phase 5 (CMIP5, Taylor et al., 2012). NorESM1-ME includes the dynamical isopycnic vertical coordinate ocean model MICOM (Bleck and Smith, 1990) and the Hamburg Oceanic Carbon Cycle model (HAMOCC5, Maier-Reimer et al., 2005), adapted to the isopycnic ocean model framework. The HAMOCC5 model simulates lower trophic ecosystem processes up to the zooplankton level, including primary production, remineralization and predation, and full water column inorganic carbon chemistry. While the simulations of NorESM1-ME are used to get a process understanding, the ESM ensemble is used to get an estimate of model uncertainty. We chose emission-driven historical and future scenarios, rather than concentration driven ones, as only those capture the full impact of carbon cycle feedbacks (Booth et al., 2013). Specifically, we utilise emission-driven historical experiments for the period from 1850 to 2005 and emission-driven future scenarios for the period from 2006 to 2100, with focus on Representative Concentration Pathways 2.6, 4.5 and 8.5 (RCP2.6, RCP4.5, and RCP8.5; Meinshausen et al., 2011; van Vuuren et al., 2011a). RCP2.6 represents a mitigation scenario, RCP4.5 a stabilization scenario and RCP 8.5 a high-emission scenario. While NorESM1-ME outputs are available for future scenarios with low to high emissions (RCP2.6, RCP4.5 and RCP8.5), the CMIP5 data-portals only contains ESM outputs for the future scenario with high emissions (RCP8.5, referred to as 'esmrcp85' within the data-portal). We therefore utilised NorESM1-ME to inform about variations in future pH-changes that are dependent on the presumed future emission strength, and our ESM-ensemble to inform about model-dependent uncertainties in those pH-changes, albeit only for the high emission scenario. Our ESM-ensemble contains all ESMs that have participated in experiment 'esmrcp85' and whose output is publicly available in one of the CMIP5 data portals and contains all variables needed for our analysis. This results in an ensemble of 7 ESMs: 1) CESM1(BGC) (The Community Earth System Model, version 1 - Biogeochemistry, Long et al., 2013), 2) CanESM2 (second-generation Canadian earth system model, Arora et al., 2011)) , 3) GFDL-ESM2G (Geophysical Fluid Dynamics Laboratory Earth System Model with Modular Ocean Model, version 4 component, Dunne et al. 2013a; 2013b), 4) GFDL-ESM2M (Geophysical Fluid Dynamics Laboratory Earth System Model with Generalized Ocean Layer Dynamics (GOLD) component, Dunne et al. 2013a; 2013b), 5) IPSL-CM5A-LR (L'Institut Pierre-Simon Laplace Coupled Model, version 5A, low resolution, Dufresne et al., 2013), 6) MPI-ESM-LR (Max Planck Institute Earth System Model, low resolution, Giorgetta et al., 2013) and 7) MRI-ESM1 (Meteorological Research Institute-Earth System Model v1, Yukimoto et al., 2011). For our model ensemble, we only investigate one realisation of each scenario.

2.1.3 Gridded climatological data

Climatological distributions of pH and Ω_{Ar} were calculated from the data of C_T, A_T, temperature, salinity, phosphate and silicate included in the mapped GLODAPv2 data product (Lauvset et al., 2016). The GLODAPv2 climatology of C_T is normalized to the year of 2002. It is important to mention that the GLODAPv2 climatology along the northern Greenland coast is mainly based on data from one cruise in 1993, and is therefore likely not representative for the long-term mean. We also

determined pre-industrial pH by subtracting the GLODAPv2 estimate of anthropogenic carbon from the mapped climatology of present C_T (Lauvset et al., 2016) for comparison with the pre-industrial state estimate from NorESM1-ME. When doing so we assumed that the changes in the temperature, salinity and A_T of the Nordic Seas are of minor importance. The GLODAPv2 estimate of anthropogenic carbon hase been calculated with the the transit time distribution (TTD). He et al. (2018) published a thorough analysis of the different sources of uncertainty in this method, and concluded that the overall uncertainty is 7.8-13.6%. Combining this with the mapping errors Lauvset et al. (2020) estimate that the global ocean anthropogenic carbon inventory calculated from the mapped fields is 167±29 PgC. Note that the GLODAPv2 mapped pre-industrial climatology is referenced to an atmospheric CO_2 level of 280 ppm, and not to a specific time period or year. These data are only used in Fig. 2.

2.1.4 Cold-water coral positions

To estimate the potential impact of the Nordic Seas acidification on cold-water corals, we used habitat positions in longitude and latitude from EMODnet Seabed Habitats (www.emodnet-seabedhabitats.eu) together with information on depth from ETOPO1 (NOAA National Geophysical Data Center, 2020).

2.2 Methods

2.2.1 Spatial drivers

To elucidate the observed spatial variability of pH and Ω_{Ar} distribution as extracted from the Nordic Seas in the GLODAPv2 climatology, we performed a correlation analysis with the drivers listed in Table 1. When it comes to C_T and A_T, one has to look at the combined effect, i.e. C_T/A_T. A potential correlation does not necessarily mean that there is a mechanistic relation, but can be a consequence of the contrasting properties of the Atlantic and polar waters. Therefore, in an attempt to better understand the effect of each driver, we calculated pH and Ω_{Ar} by step by step introducing the spatially varying climatologies of the drivers, while keeping all other drivers constant (set to the spatial mean value of the Nordic Seas surface waters). First, we calculated pH and Ω_{Ar} by using the spatially varying temperature climatology, and keeping all other variables constant (pH(T), Ω_{Ar}(T)). Thereafter, we repeated the same exercise with the spatially varying temperature, C_T and A_T climatologies to get pH(T, C_T, A_T) and Ω_{Ar}(T, C_T, A_T). Finally, we added the salinity variability to get pH(T, C_T, A_T,S) and Ω_{Ar}(T, C_T, A_T, S). We started with temperature because it has an initial thermodynamic effect on pH and Ω_{Ar}, and a subsequent, secondary, effect from the resulting air-sea CO_2 exchange and change in C_T/A_T. Salinity was chosen as the last variable due to the minor effect it has on pH and Ω_{Ar}.

2.2.2 pH changes and its drivers

It is important to keep in mind that changes in pH represents a relative change, and that pH trends are therefore not directly comparable across water-masses with large differences in mean pH (Fassbender et al., 2021). In these cases, it is preferable to evaluate changes in H^+ concentration that represents an absolute change (Kwiatkowski and Orr, 2018). However, pH variations in the Nordic Seas are relatively small, and we have therefore decided to use pH in this study.

Present

Measurements of C_T, A_T, temperature, salinity (Figs. S1-S4) phosphate and silicate from the data sets described in Sect. 2.1.1 were used to calculate pH (on total scale) and Ω_{Ar}, at in situ temperature and pressure, using CO2SYS for MATLAB (Lewis and Wallace, 1998; van Heuven et al., 2011). Wherever nutrient data were missing, silicate and phosphate concentrations were set to 5 μmol kg^{-1} and 1 μmol kg^{-1}, respectively. For the CO2SYS calculations we used the dissociation constants of Lueker et al. (2000), the bisulfate dissociation constant of Dickson (1990) and the borate-to-salinity ratio of Uppström (1974). This ratio has recently been shown to be suitable for the western Nordic Seas (Ólafsson et al., 2020a).

Present day trends (1981-2019) in pH, and Ω_{Ar} were determined for six different regions in the Nordic Seas: the Norwegian Basin (NB), the Lofoten Basin (LB), the Barents Sea Opening (BSO), Eastern Fram Strait (FS), the Greenland Sea (GS) and the Iceland Sea (IS) (Fig. 1). These regions were chosen not only based on the data-availability (they are centered around stations and sections where repeated measurements are taken), but also in order to get a representation of the main surface water-masses of the Nordic Seas. The Norwegian Basin, Lofoten Basin, and Barents Sea Opening are all under the influence of relatively warm and salty northward flowing Atlantic Water, while the Greenland and Iceland seas are more influenced by relatively cold and fresh southward flowing polar waters. The Fram Strait is an area that in the surface is under influence of Atlantic Water in the eastern part, and polar waters in the western part. In order to minimize the aliasing effects of latitudinal and longitudinal gradients, the geographical range of each region was kept as small as possible. For example, the boundaries of the Fram Strait box are constrained to the east, in order to ensure that this mostly represents the influence of Atlantic Waters, and we therefore refer to is as the Eastern Fram Strait. Regional trends were computed from annual means for five different depth intervals (0-200, 200-500, 500-1000, 1000-2000, and 2000-4000 m) using linear regression. Although summer mixed layer depths generally is shallower than 200 m, a thickness of 200 m was used for the surface layer since this sets the approximate limit for the influence of seasonal variations associated with, e.g., primary production (e.g. Skjelvan et al., 2008). The significance of the trends (at 95% confidence level), were determined from the p-value of the t-statistic, (as implemented in MATLAB's fitlm function). For the comparison of trends, we determined 95% confidence intervals of the slopes by the use of the Wald method (as implemented in MATLAB's fitlm and coefCI functions).

The observed long-term changes in pH were decomposed into contributions from changes in temperature (T), salinity (S), C_T and A_T (Figs. S1-S4), following the proceedure of Lauvset et al. (2015). First, the effect of each of these processes on the CO_2 fugacity (fCO_2) is determined following Takahashi et al. (1993) and Metzl et al. (2010):

$$\frac{dfCO_2}{dt} = \frac{\partial fCO_2}{\partial T}\frac{dT}{dt} + \frac{\partial fCO_2}{\partial S}\frac{dS}{dt} + \frac{\partial fCO_2}{\partial C_T}\frac{dC_T}{dt} + \frac{\partial fCO_2}{\partial A_T}\frac{dA_T}{dt} \tag{7}$$

Second, the magnitude of each fCO_2 driver is converted to [H^+] by using Henry's law ([CO_2] = $k_0 \times fCO_2$) and the expression for d[H^+]/d[CO_2] (equation 1.5.87 Zeebe and Wolf-Gladrow, 2001):

$$\frac{d[H^+]}{dt} = \frac{d[H^+]}{d[CO_2]}\frac{k_0 \times dfCO_2}{dt} \tag{8}$$

Finally, we converted it to pH by acknowledging that dpH = -([H^+]ln(10))$^{-1}$d[H^+].

We additionally made a decomposition of the A_T and C_T drivers into a freshwater component and a biogeochemical component (Supplementary material, Sect. 1). The freshwater drivers of A_T and C_T are typically of similar magnitude and opposite sign, and consequently cancel each other. We therefore decided to stay with the more simple decomposition as shown in Eq. 7. The only exception is discussed in Sect. 4.1.

To understand whether the observed pH changes are consistent with the changes in atmospheric CO_2, the pH change that can be expected in seawater where the pCO_2 perfectly tracks the atmospheric pCO_2 (pH_{perf}) was determined for each region by adding the observed change in atmospheric xCO_2 to the local mean pCO_2 for the first year with observations, and then calculating the pH with CO2SYS with the local temperature, salinity, A_T, phosphate and silicate and their respective changes as inputs. We did not make any corrections for water vapour and atmospheric pressure because the rates of change for xCO_2 and pCO_2 are the same. Any deviation between observed pH change and pH_{perf} is a consequence of changes in seawater pCO_2 that are smaller/larger than in the atmosphere, i.e a change in the air-sea pCO_2 difference.

Past and future

As described in Sect. 1.1, the total change in pH and saturation states does not only depend on local changes in C_T, A_T, temperature, salinity, and nutrients, but also on the initial buffer capacity of the seawater. ESMs are usually biased, i.e., there is an offset between modelled fields and reality. In particular, NorESM1-ME has high A_T and low C_T relative to observations in deep waters, leading to a biased high pH (Fig. S5) and saturation states (not shown). To alleviate this bias in our analysis of past and future pH and Ω_{Ar}, we applied the modelled rates of change of temperature, salinity, C_T, A_T, phosphate and silicate to the gridded GLODAPv2 climatology. From this we obtained past and future states of these properties, which were used to calculate the past and future pH, Ω_{Ar} and Ω_{Ca} in CO2SYS. Similar procedures have been used by Orr et al. (2005) and Jiang et al. (2019) for the calculation of future pH. The modelled rates of change from present to future and past to present were calculated as the difference between the time period of 2090-2099 and 1996-2005, and 1996-2005 and 1850-1859 (10-year means), respectively. Because the historical runs end at 2005, and thereafter are branched into future scenarios, we could not center our 10 year means around 2002, the year to which the GLODAPv2 climatology is normalized.

The methodology for calculating pH drivers described in the previous section was also used for calculating the drivers of past (1850-1859 to 1996-2005) and future (1996-2005 to 2090-2099) pH changes, using the changes in temperature, salinity, A_T and C_T data from NorESM1-ME output together with the climatological values from GLODAPv2.

2.2.3 Uncertainty analysis

There are several sources of uncertainties (σ) involved in our calculations of pH and Ω: measurement uncertainty (σ_{mes}), mapping uncertainty (σ_{map}) for the gridded product, and uncertainties related to dissociation constants (σ_{Kx}) used in the CO2SYS calculations. To estimate the total uncertainties in pH and Ω resulting from these we used the uncertainty propagation routine in CO2SYS (Orr et al., 2018). The uncertainties in the input parameters (A_T, C_T, temperature, salinity, phosphate

and silicate) were set to σ_{mes} for the single measurements, and $\sqrt{\sigma_{mes}^2 + \sigma_{map}^2}$ for the mapped product and for the past and future estimates. As σ_{mes} we used the estimated uncertainties from Olsen et al. (2019), and for σ_{map} we used the mapping uncertainty (3D field) from Lauvset et al. (2016). The correlation between uncertainties in A_T, C_T were set to 0. Including a correlation term would decrease the uncertainty, and possibly overestimating the uncertainty is preferable to including a poorly constrained correlation term (Lauvset et al., 2020). For the dissociation constants we used the default uncertainties in CO2SYS. From here on, the calculated uncertainties will be presented as σ_1, when σ_{Kx} and σ_{mes} are included, and σ_2, when σ_{Kx}, σ_{mes} and σ_{map} are included.

For the observations described in Section 2.1.1, the mean, maximum and minimum uncertainties (σ_1) in pH, Ω_{Ar}, Ω_{Ca} and pCO_2 obtained from the uncertainty propagation are listed in Table 2. Variations in the uncertainties arise from variations in temperature and salinity, which impact the uncertainty of dissociation constants. As discussed in Orr et al. (2018), random and systematic uncertainties tend to cancel out when calculating trends (i.e. comparing measurements from the same location but from different times), unless there are substantial changes in the local salinity and temperature. Therefore, to estimate to what extent these uncertainties could impact our trend estimates, we investigated whether there is any trend in the uncertainties (Figs. S6-S7).

Table 2. Uncertainties (σ_1, mean, max and min) in pH, Ω_{Ar}, Ω_{Ca} and pCO_2 (μatm), calculated from the individual observations described in Section 2.1.1.

	mean	max	min
pH	0.017	0.022	0.014
Ω_{Ar}	0.085	0.174	0.037
Ω_{Ca}	0.134	0.271	0.058
pCO_2	14.387	53.608	5.901

In our observational data, there is also an uncertainty in the annual mean estimates related to seasonal undersampling. Most samples (about 60% in total) from the data sets described in Sect. 2.1.1 were collected during spring and summer (April-September, Figs. S8-S13). The uneven sampling frequency of different seasons introduces uncertainty in the annual means of the uppermost ocean layer, and can bias the trend estimates. Unfortunately, there are not enough data to allow for deseasonalization in order to remove such potential biases. To get an idea of the effect of seasonal undersampling we additionnaly calculated trends by using annual means containing samples from April-September, and June-August, only.

Because a large part of this study focuses on process understanding and the driving factors behind pH change, we do not consider model uncertainty in Sect. 3, where the drivers of pH change in the model projections are analysed, here we only use the combined uncertainties of measurements and mapping.

In Sect. 4.2, where the future aragonite saturation horizon is presented, we additionally take into account model and scenario uncertainty. Modelled future projections are uncertain due to incomplete understanding or parameterization of fundamental processes, as well as different and unknown future carbon emission scenarios (Frölicher et al., 2016). We note that internal climate variability is an additional source of uncertainty that we do not take into account in this study. The model dependent

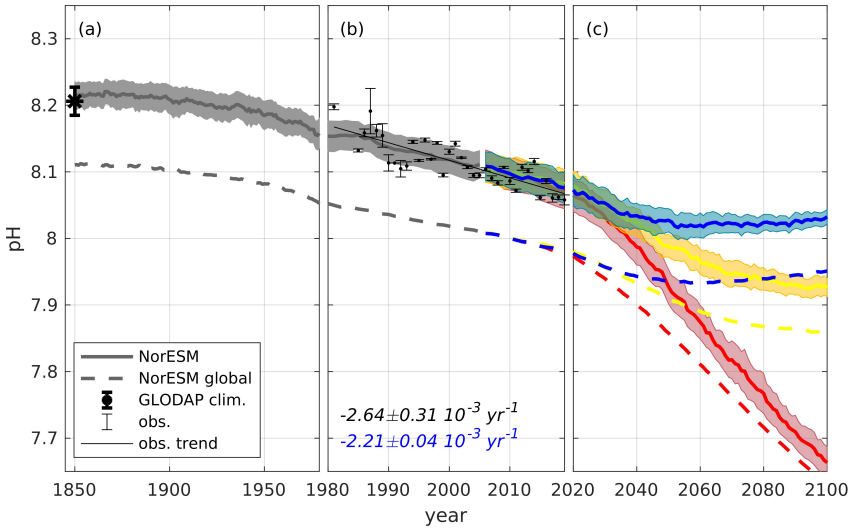

Figure 2. pH evolution, averaged over the Nordic Seas surface waters (0-200 m), from 1850 to 2100, separated into past (1850-1980), present (1981-2019) and future (2020-2100). Black dots with error bars show the observed annual mean pH, with standard deviations (due to spatial/seasonal variations), determined from all available observations in the Nordic Seas shown in Fig. 1. The solid black line shows the trend calculated from the observations. The gray, red, yellow and blue solid lines show NorESM1-ME output for emission-driven historical and future (RCP8.5, RCP4.5 and RCP2.6) simulations, respectively, where the shading depicts the spatial variation (standard deviation). Note that this figure illustrates the actual modelled pH data, and not the modelled rates of change applied to observational data. The dashed lines show the evolution of global surface ocean pH from the same simulations. The black asterisk (1850) with error bars show an estimate of the pre-industrial mean pH with spatial standard deviation, derived from the GLODAPv2 mapped product as described in Sect. 2.1.3. The numbers in black and blue show the calculated and significant linear trend with standard errors from the observations and the model, respectively, for the period of 1981-2019.

uncertainty of the future saturation horizon, under the emission-driven RCP8.5 scenario, is estimated by adding the modelled change in C_T and A_T for each model of our ESM-ensemble to the GLODAPv2 climatologies. Here we neglect the changes of temperature, salinity, phosphate and silicate because they are minor in comparison to the effect of the changes in C_T and A_T (Sect. 4.1).

3 Results

Before going into regional details of pH changes, we will give an overview of surface pH changes from 1850 to 2100 (Fig. 2). To be consistent with our regional analysis in Sect. 3.3, the surface layer is taken as the top 200 m. The pre-industrial estimates of the average Nordic Seas surface pH in GLODAPv2 and NorESM1-ME (from year 1850) are in good agreement (within the spatial standard deviations), with mean values of 8.21±0.02 and 8.22±0.02, respectively. From 1850 to 1980, NorESM1-

ME simulates an average pH decline of 0.06 in the Nordic Seas. For the period between 1981 and 2019, the modelled pH encompasses the observed one (within the spatial standard deviations), except for a few years, showing that the pH of the Nordic Seas surface water is reasonably well simulated. The pH trend estimated from the observations for this period, -2.64±0.31 10^{-3} yr^{-1}, is not significantly different (at the 95% confidence level) from the modelled pH trend, -2.21±0.04 10^{-3} yr^{-1}. Because the pH calculated from observational data is based on discrete samples with incomplete spatial and temporal coverage, its representatives for the entire Nordic Seas can be questioned, and we cannot expect an exact agreement with the model.

As expected, the future evolution of surface water pH in the Nordic Seas depends strongly on the CO_2 emission scenario (Fig. 2). Under the high-CO_2 emission RCP8.5 scenario, NorESM1-ME simulates the pH to decrease by 0.40 between 2020 and 2100, to an average value of 7.66±0.02 by the end of the century (model ensemble range: 7.59-7.79, Fig. S5). For the RCP4.5 scenario, which corresponds roughly to the currently pledged CO_2 emission reductions under the Paris agreement, the surface pH is simulated to drop by about 0.15, reaching an average value of 7.93±0.01. In the RCP2.6 scenario, where the CO_2 emissions are kept within what is needed to limit global warming to 2 °C (van Vuuren et al., 2011b), pH reaches its lowest value of 8.02±0.02 in the middle of the century, before it increases again to reach a value of 8.03±0.01 by the end of the century. This peak and decline is related to the overshoot profile of the atmospheric CO_2 concentration, with a maximum value of 443 ppm in mid-century followed by net negative emissions that subsequently decrease the atmospheric CO_2 down to 421 ppm in 2100.

In 1850, the simulated Nordic Seas average surface pH is 0.11 units higher than the global average, which is related to the undersaturation of CO_2 in the surface waters of the Nordic Seas (Jiang et al., 2019). Note that our global average is lower than the one estimated by, e.g., Jiang et al. (2019) for the surface ocean due to our 200 m thick surface layer. The difference between the global ocean and the Nordic Seas is decreasing with time and by the end of the century the Nordic Seas surface pH is 0.03, 0.07 and 0.08 pH units higher than the global average in the RCP8.5, RCP4.5 and RCP2.6 scenarios, respectively. This is most likely partly due to the colder waters of the Nordic Seas, which gives them a lower buffer capacity, and partly due to a faster warming in the high latitude oceans related to polar amplification (Dai et al., 2019), which would give a faster decrease in the Nordic Seas pH compared to the global mean. Additionally, in RCP8.5, there is an increase in the pCO_2 undersaturation of the global ocean that increases the global average pH (Fig. S14).

3.1 Present distribution of pH and Ω saturation states

Due to the contrasting properties of the Atlantic waters (here defined as waters with salinity>34.5) and polar waters (salinity<34.5) that meet and mix in the Nordic Seas, there are large spatial gradients in its surface temperature, salinity and chemical properties (Fig. S15). The Atlantic Water, located in the eastern part of the Nordic Seas, is characterized by higher temperature, salinity, and A_T, while polar waters are colder and fresher with lower A_T. This results in a decrease in temperature, salinity, and A_T from south and east to north and west. Within the Atlantic water, C_T increases with decreasing temperature, largely as a consequence of the increased CO_2 solubility in colder water. The C_T associated with polar waters is lower than that of Atlantic waters.

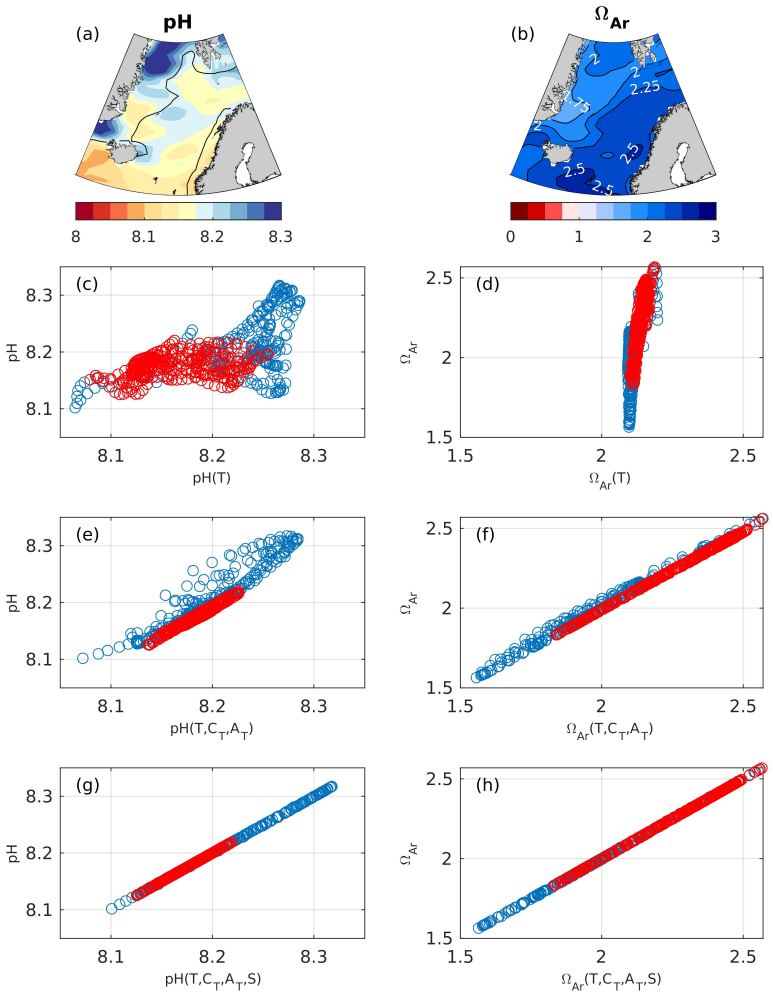

Figure 3. Maps of present day surface pH (a) and Ω_{Ar} (b). The solid line in (a) mark the the border between Atlantic Water (salinity>34.5) and polar waters (salinity<34.5). pH and Ω_{Ar} plotted against variations induced by temperature (c,d), temperature and C_T/A_T (e,f) and temperature, C_T/A_T and salinity (g,h) in pH and Ω_{Ar}, calculated as described in Section 2.2.1 in Atlantic Water (red) and polar waters (blue). Each circle represents a value from a single grid.

340 The pH in the Nordic Seas increases from the Atlantic waters to the polar waters (Fig. 3). There is a significant, strong (R<-0.5), negative correlation with all drivers, i.e. pH decreases with increasing temperature, salinity, C_T and A_T (Table 3 and Fig. S16). Here, only the negative correlation with A_T is nonphysical, i.e. we would expect an increasing pH with an increasing A_T (Table 1). The correlation with C_T/A_T is insignificant. Because the drivers are not orthogonal, it is impossible to rule out

the contribution of each driver by just looking at these correlations, and we can only conclude that there is a strong water-mass dependency in the spatial distribution of these variables.

From the correlation between the pH and pH(T), we note that temperature-induced variations (through the thermodynamic effect) are able to explain 34% of the spatial variability in pH (Fig. 3). The range in pH(T) values (8.06 - 8.29) is very close to the observed one (8.10-8.32), indicating that temperature alone can give rise to the observed pH-range. Adding C_T and A_T to the picture explains an additional 55% (temperature, C_T and A_T explain all together 89%), and are therefore important contributors to spatial variations in pH, in contrast to what is suggested by directly correlating these variables (Table 3). This shows that the influence of C_T and A_T on pH is masked out by temperature variations in Table 3 and Fig. S16, which can be explained by the two cancelling effects that temperature has on pH described in Jiang et al. (2019). For example, while the instantaneous, thermodynamic, effect of a drop in temperature leads to a pH increase, it also gives rise to a decrease in pCO_2 that leads to a CO_2 uptake from the atmosphere, which subsequently increases the C_T/A_T ratio and decreases the pH. In the Nordic Seas, the spatial pH variations strongly correlate with surface pCO_2 (R=-0.99, Table 3), which range between 185 and 342 μatm and is lower than the atmospheric pCO_2 of 373 μatm (in year 2002, to which these data are normalized). This undersaturation is partly a result of the large heat release to the atmosphere and cooling of the sea surface, and shows that the sea surface CO_2 did not yet equilibrate with the atmosphere. Because most of the data have been used to produce these climatologies are from the productive season, there is probably also a contribution from primary production to this undersaturation. There is also a negative correlation between C_T/A_T ratio and temperature, indicating that CO_2 uptake has been taking place. The temperature effect on pH in the Nordic Seas is therefore a combination of the instantaneous thermodynamic effect, and the effect of the subsequent CO_2 exchange and the resulting increase in the C_T/A_T ratio. The strong relation between pH and pCO_2, which also has been observed for the global ocean (Jiang et al., 2019), suggests that the processes responsible for the spatial pH variations in the Nordic Seas are heat fluxes and production/remineralization of organic matter. On top of temperature, C_T and A_T, the addition of salinity explains the last 11% of the spatial variability in pH. The effect of salinity is the largest in the low-saline regions, i.e in the polar waters and in the Norwegian coastal current.

The Ω_{Ar} show an opposite pattern to pH, with low saturation states in polar waters, and high saturation states in Atlantic Water. The Ω_{Ar} distribution is strongly correlated with C_T/ A_T (R=-0.99) (Fig. 3,f) and temperature (R=-0.86). This is related to the strong relation between Ω_{Ar} and C_T/ A_T to the climatological temperature distribution and its impacts on the CO_3^{2-} concentration (for which C_T/ A_T is a proxy), as described in Section 1.1. As for pH, temperature has two effects on Ω_{Ar}, but in contrast to pH where these effects are counteracting, they reinforce each other for Ω_{Ar}. From Fig. 3,d, it becomes clear that the temperature effect on the solubility of Ω_{Ar} (Ω_{Ar}(T)) only can explain 11% of the observed Ω_{Ar} range, although it is able to explain 98% of the variability. The strong correlation with temperature is therefore largely a result of the temperature effect on C_T/ A_T (Sect. 1.1 and Orr (2011); Jiang et al. (2019)). When adding C_T/ A_T to the picture, the observed range in Ω_{Ar} is reproduced, and 100% of the variability is explained. Salinity induced variations only have a minor contribution to the spatial variations in Ω_{Ar}. As for pH, the effect of salinity is more prominent in the low salinity-regions.

Table 3. Spatial correlation between various chemical and physical properties in the Nordic Seas surface waters. Numbers in bold indicate significant correlation.

	pH	Ω_{Ar}	pCO_2	C_T/A_T
Temperature	**-0.58**	**-0.86**	**0.66**	**-0.79**
Salinity	**-0.68**	**0.46**	**0.71**	**-0.35**
C_T	**-0.75**	-0.07	**0.74**	0.07
A_T	**-0.64**	**0.63**	**0.69**	**0.5**
C_T/A_T	-0.02	**-0.99**	-0.09	
pCO_2	**-0.99**	**-0.23**		

Table 4. Spatial correlation (r) and explained variance (r^2, in paranthesis) between pH and pH(T), pH(T,C_T,A_T) and pH(T,C_T,A_T, S), and between Ω_{Ar} and Ω_{Ar}(C_T,A_T), Ω_{Ar}(C_T,A_T, T) and Ω_{Ar}(C_T,A_T, T, S) in the Nordic Seas surface waters. Numbers in bold indicate significant correlation.

Drivers	pH(T)	pH(T,C_T,A_T)	pH(T,C_T,A_T,S)
pH	**-0.58** (0.34)	**-0.94** (0.89)	**1.00** (1.00)
Drivers	Ω_{Ar}(T)	Ω_{Ar}(T,C_T,A_T)	Ω_{Ar}(T,C_T,A_T,S)
Ω_{Ar}	**0.85** (0.73)	**1.00** (1.00)	**1.00** (1.00)

3.2 Changes from pre-industrial to present

Maps of surface pH and Ω_{Ar} distributions, and their changes from pre-industrial to present (calculated from the gridded GLODAPv2 data and rates of change from the NorESM1-ME emission-driven historical run as described in Section 2.2.2), are shown in Fig. 4. The spatial pattern of changes in pH and Ω_{Ar} are similar. The strongest decreases, reaching -0.12 and -0.55, respectively, are found in Atlantic waters along the Norwegian coast both for pH and Ω_{Ar}. The smallest change is found in polar waters. The reasons behind these patterns of change will be discussed in Section 4.1.

Due to the longer ventilation time scales of deeper waters, the pH decrease weakens with depth. As shown in the section across 70°N (Fig. 5) waters below 2500 m are nearly unaffected. While the entire water column remains saturated with respect to calcite, the saturation horizon (Ω=1) of aragonite shoaled from a mean depth of 2200 m (uncertainty range: 2100-2400) during pre-industrial, to a mean depth of 2000 (uncertainty range: 1700-2300) m in present times, across this specific section. Note that these depths were obtained from the contour interpolation when creating Fig. 5, which has a finer vertical resolution than the GLODAPv2 climatology.

3.3 Present day changes (1981-2019)

Regional trends in observed seawater pH between 1981 and 2019 for the five different depth intervals are presented in Fig. 4.1 and Table 5. The corresponding trends in H^+ are shown in Fig. S17 and Table S7. In surface waters (0-200), significant

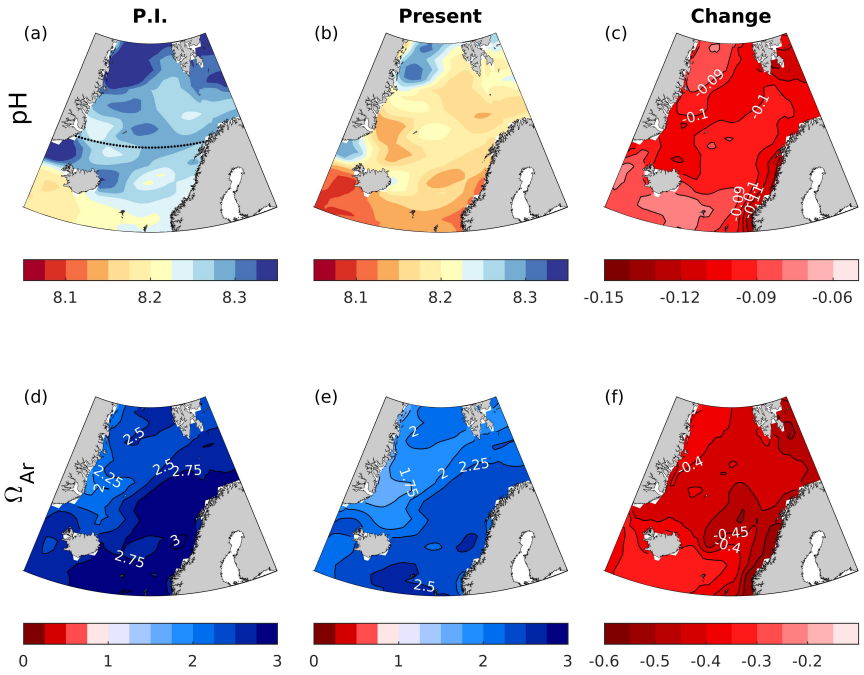

Figure 4. Maps of surface water pH and Ω_{Ar} for pre-industrial (P.I., 1850-1859) , present times (1996-2005), and the change in between the two periods. The maps were calculated from the GLODAPv2 gridded climatologies (Lauvset et al., 2016) applying the simulated changes by NorESM1-ME, as explained in Sect. 2.2.2. The dotted black line in (a) show the location of the crossection presented in Fig. 5.

Table 5. pH trends ± standard error (10^{-3} yr^{-1}) calculated from the data presented in Fig. 4.1. Bold numbers indicate that the trends are significantly different from zero.

Depth (m)	NB	LB	BSO	FS	GS	IS
0-200	**-3.04±0.32**	**-2.4±0.23**	-1.67±0.77	**-2.53±0.74**	**-2.19±0.37**	**-3.1±0.30**
200-500	**-2.22±0.32**	**-1.89±0.31**	-1.05±0.82	**-1.49±0.42**	**-1.61±0.22**	**-2.51±0.27**
500-1000	**-1.17±0.27**	**-2.27±0.46**		-1.09±0.52	**-1.52±0.18**	**-1.84±0.29**
1000-2000	**-0.65±0.22**	-0.8±0.40		-0.55±0.81	**-1.36±0.15**	**-1.3±0.21**
2000-4000	0.46±0.55	-0.22±0.51		-0.03±0.69	-0.31±0.23	

trends of 2-3 10^{-3} yr^{-1} are found in all basins except for the Barents Sea Opening. The uncertainties (standard errors) of these trends are approximately between ±0.3 and ±0.8 10^{-3} yr^{-1}. Due to the difference in sampled years, we cannot robustly compare the magnitude of trends between the basins. The estimated trend in the Norwegian Basin of -3.04 ± 0.32 10^{-3} yr^{-1} is weaker than the -4.1 10^{-3} yr^{-1} trend estimated for the period 1981-2013 by Skjelvan et al. (2014), which can be a result

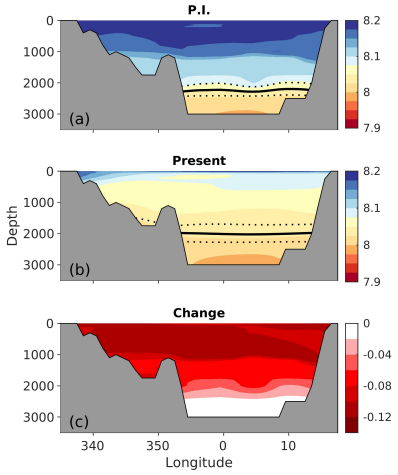

Figure 5. Zonal cross sections (at 70 °N) of pre-industrial (1850-1859) and present pH (1996-2005), and the change between the two periods. The solid black line shows the saturation horizon of aragonite (Ω_{Ar}=1). The dashed lines shows the associated uncertainties(σ^2).

of different sampling period and slightly different definition of regions. However, our trend estimate in the Greenland Sea of -2.19 $\pm$ 0.37 10^{-3} yr^{-1} agrees well with their trend of -2.3 10^{-3} yr^{-1}. As expected from the generally longer ventilation time scales of deep waters, the trends in pH declines with depth (but see Sect. 3.4). Significant trends are detected down to 2000 m in the Norwegian Basin, and in the Greenland and Iceland seas. In the Lofoten Basin and Eastern Fram Strait, however, the decrease in pH is significant down to the 1000 m and 500 m layers, respectively. In the shallow Barents Sea Opening there is no significant trend below the surface layer.

Trends of aragonite saturation states are shown in Fig. 7 and Table 6. As for pH, the rates of change is strongest in surface waters. For Ω_{Ar}, the rates of decline are in the order of 10^{-2} yr^{-1} and significant in all regions except for the Greenland Sea. The weak decline in the Greenland Sea surface layer is a result of a smaller increase in C_T in combination with relatively strong increases in A_T and temperature, which counteracts the effect of C_T on the saturation states (while the temperature amplifies pH declines, see Sect. 4.1). The reduction in Ω_{Ar} is significant down to 2000 m in the Norwegian Basin and the Greenland and Iceland seas. In the other regions no significant decline has occurred below the surface layer. The waters in the depth range 1000-2000 m are close to the limit of undersaturation. The smallest values in this layer are 1.05, 1.07, 0.99, 1.02, for the Norwegian Basin, Lofoten Basin, Barents Sea Opening, Eastern Fram Strait, Greenland Sea and Iceland Sea, respectively. Considering the associated uncertainties of 0.06 (Table 2), this is indistinguishable from undersaturation in all regions except for the Lofoten Basin. Only the waters between 2000-4000 m, which are already undersaturated in aragonite, are more or less unaffected.

During this period of time we detect trends in the uncertainties of pH and Ω_{Ar} (Figs. S6 and S7). These are, however, about two orders of magnitude smaller than the trends pH and Ω_{Ar}, and they do therefore not significantly impact our estimated trends.

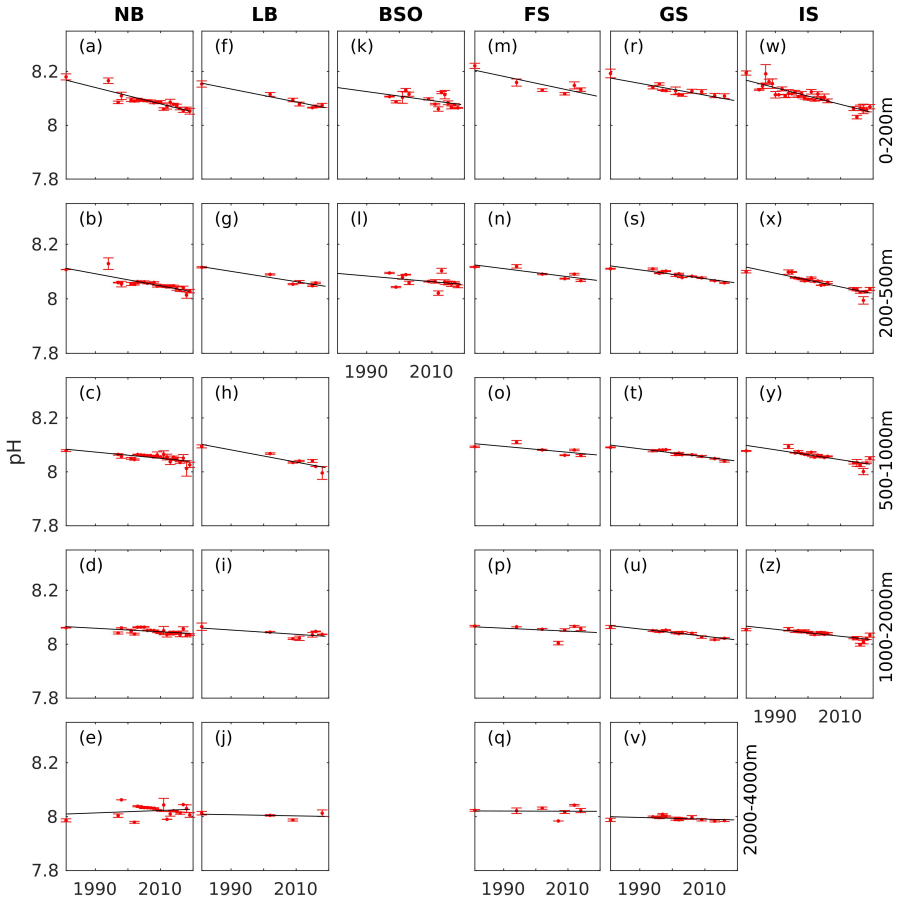

Figure 6. Annual mean pH (red dots) with standard deviation (error bars) in the different basins, at five different depth levels, calculated as described in Sect. 2.2.2. The solid black line show the trend estimate from the linear regression.

Table 6. Ω_{Ar} trends $\pm$ standard error (10^{-3} yr^{-1}) calculated from the data presented in Fig. 7. Bold numbers indicate that the trends are significantly different from zero.

Depth (m)	NB	LB	BSO	FS	GS	IS
0-200	**-11.97±3.25**	**-8.45±1.18**	**-8.29±3.54**	**-11.61±3.13**	-4.05±3.21	**-11.20±2.22**
200-500	**-5.57±2.51**	-1.76±2.17	3.94±3.01	-2.06±1.60	**-3.19±0.61**	**-6.37±0.74**
500-1000	**-4.28±1.25**	-5.55±3.38		-1.11±1.46	**-2.98±0.52**	**-4.52±0.71**
1000-2000	**-3.49±1.24**	0.03±1.76		0.65±3.08	**-2.98±0.59**	**-2.57±0.50**
2000-4000	3.67±1.82	0.33±1.57		1.13±1.53	0.53±0.80	

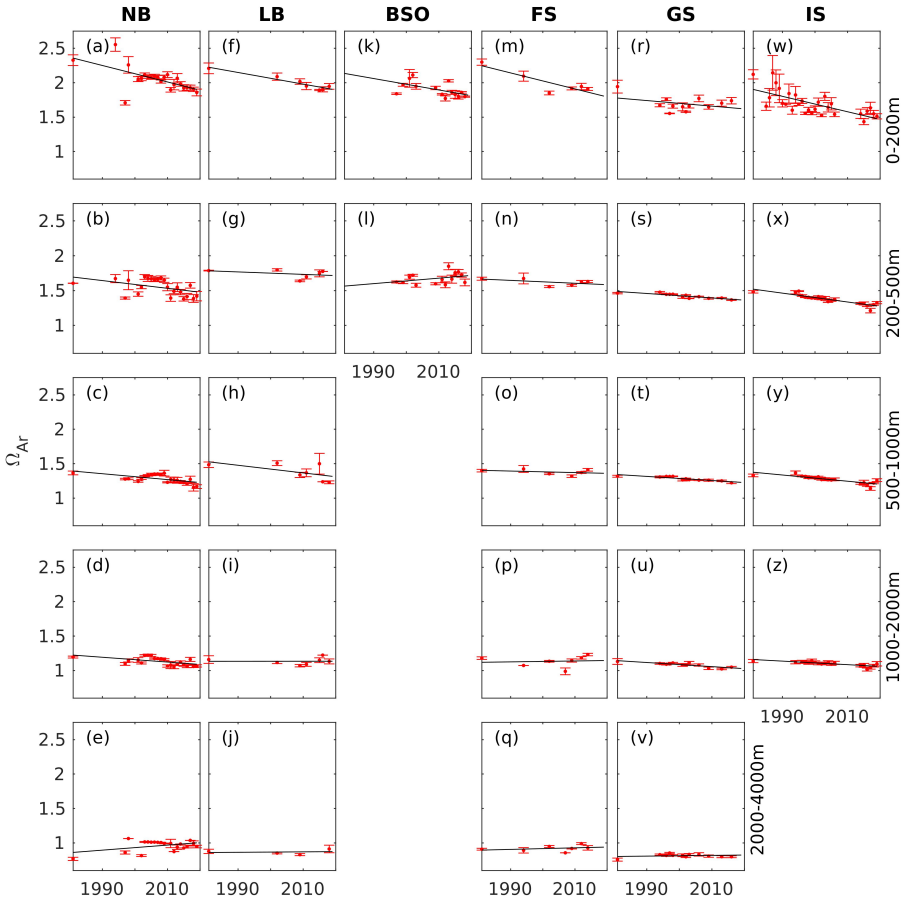

Figure 7. Annual mean Ω_{Ar} (red dots) with standard deviation (error bars) in the different basins, at five different depth levels, calculated as described in Sect. 2.2.2.The solid black line show the trend estimate from the linear regression.

3.4 Future changes

The future evolution of pH in the Nordic Seas depends strongly on the emission scenario (Fig. 2). Here we will present, in more detail, the future evolution of pH and Ω_{Ar} under low and high emission scenarios, RCP2.6 and RCP8.5 respectively, as simulated by NorESM1-ME.

420 In RCP2.6, an additional pH decline of 0.06-0.11 in the surface waters is simulated between present (1996-2005) and future (2090-2099) (Fig. 8c). The largest pH decreases are found in polar waters, leading to a weakening of the zonal gradient in pH that we see in the present and pre-industrial periods. The surface Ω_{Ar} is expected to decrease by about 0.2-0.5. Surface waters are expected to remain supersaturated with respect to both calcite and aragonite under RCP2.6. An interesting feature in this scenario, is that the strongest ocean acidification occurs at depths of 1000-2000 m (Fig. 9c), which leads to a shoaling of the

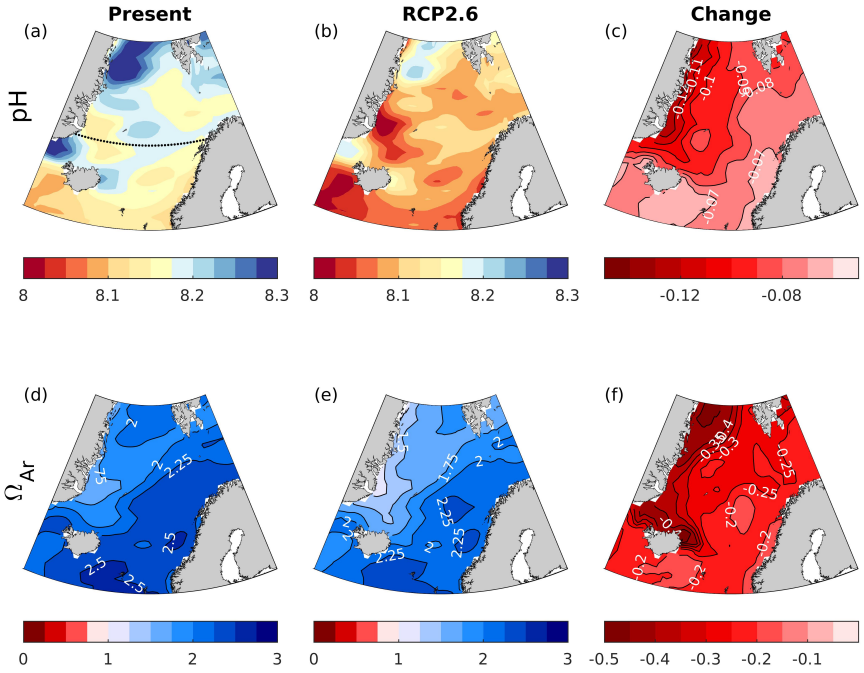

Figure 8. Maps of surface water pH and Ω_{Ar} for the present (1996-2005) and the RCP2.6 future (2090-2099), as well as the changes between the periods. The maps are drawn from the GLODAPv2 gridded climatologies combined with rates of change from the NorESM1-ME.The dotted black line in (a) show the location of the crossection presented in Fig. 9.

aragonite saturation horizon to a depth of 1100 m (uncertainty range: 800-1200 m). This is discussed in more detail in Sect. 4.1.

Under the RCP8.5 scenario, the pH in surface waters drops by about 0.4-0.5 from present, to a value of 7.6-7.9 in 2100 (Fig. 10), with the largest decreases taking place in polar waters. The surface Ω_{Ar} drop by around 1.1-1.3. In contrast to RCP2.6, the largest decline take place in the Atlantic Water. The strong ocean acidification in this scenario leads to a reversal of the pH depth dependency so that by the end of the century pH increases from the surface to deep ocean (Fig. 9c), reflecting that the input of anthropogenic carbon at the surface overrides the effect of pressure and organic matter remineralization on the vertical pH gradient. The change in Ω_{Ar} is large enough to bring the entire water column, and consequently also the entire seafloor, to aragonite undersaturation. The only exception is a thin surface layer (above 30 $\pm$10 m) in the Atlantic Water region.

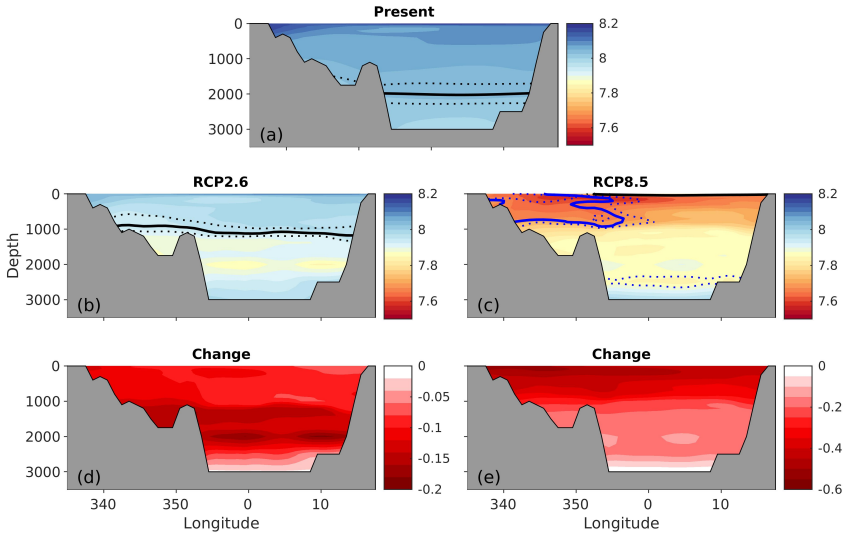

Figure 9. Zonal cross sections (at 70 °N) of the present (1996-2005) and future (2090-2099) pH under the emission-driven RCP2.6 and RCP8.5 scenarios, along with the change between the periods. The solid and dotted black lines show the saturation horizon of aragonite (Ω_{Ar}=1) with uncertainty (σ2). The solid and dotted blue line show the corresponding for calcite (Ω_{Ca}=1).

4 Discussion

4.1 Drivers of Ocean Acidification

To understand what has caused the pH changes presented in Sect. 3, we decompose the trends into their different drivers using Eq. 2 and subsequent transformation of fCO_2 to pH (Fig. 11). In the surface layer (i.e. the upper 200 m) the pH decrease is in agreement (within 95% confidence) with the pH change expected from the increase in atmospheric CO_2, except in the Norwegian Basin and the Iceland Sea where the trends are larger. This is related to a faster increase in the seawater pCO_2 compared with that of the atmosphere (Fig. S18), meaning that the pCO_2 undersaturation of the Norwegian Basin and the Iceland Sea is diminishing. The significance of these results are, however, sensitive to the choice of months, i.e., trends calculated with data from April-September, or July-August, give different results. The strong positive trend in pCO_2 that we see in our dataset can therefore be a result of seasonal undersampling, and should be verified with a larger dataset. Notwithstanding, diminishing pCO_2 undersaturation have been observed in earlier studies of the North Atlantic (Lefèvre et al., 2004; Olsen et al., 2006; Ólafsson et al., 2009; Metzl et al., 2010; Skjelvan et al., 2014), and could be a result of a change in any of the mechanisms underlying the pCO_2 under saturation in surface waters of the Nordic Seas (see Sect. 1), including cooling of northward flowing Atlantic waters, primary production and the outflow of pCO_2 undersaturated waters from the Arctic Ocean. Considering that the data we have used are biased towards the productive season, it is possible that parts of the increase in the degree of pCO_2 saturation comes from a reduction in the efficiency of the biological pump (i.e. biological

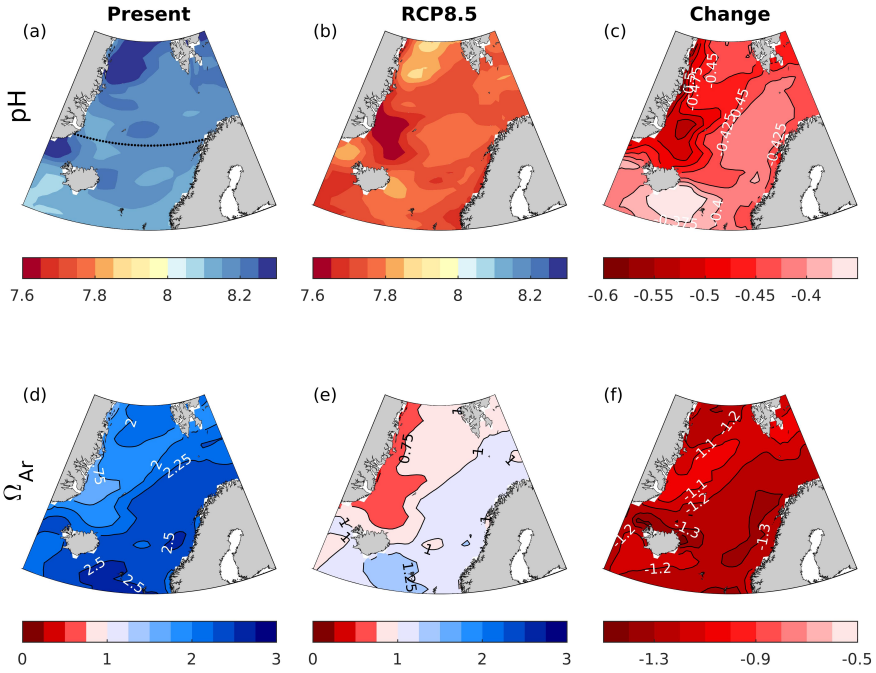

Figure 10. Maps of surface water pH and Ω_{Ar} for the present (1996-2005) and the RCP8.5 future (2090-2099), as well as the changes between the periods. The maps are drawn from the GLODAPv2 gridded climatologies combined with rates of change from the NorESM1-ME. The dotted black line in (a) show the location of the crossection presented in Fig. 9.

CO_2 consumption). Lefèvre et al. (2004) observed a stronger increase in the seawater pCO_2 during summer compared with winter in the North Atlantic subpolar gyre, which they suggested to be a result of a decrease in productivity. One other possible mechanism was suggested in Olsen et al. (2006) and Anderson and Olsen (2002), where they associated the fast increase in seawater pCO_2 with a large advective supply of anthropogenic carbon from the south and corresponding changes in the buffer capacity (see also Terhaar et al. (2020b)).

The main driver of the pH decrease in the surface layer is increasing C_T, which is partly offset by A_T increases (see also Fig. S4). The effect of increasing A_T is strongest in the Barents Sea Opening that, together with an apparent cooling, explain the low, non-significant, pH decline observed there (Fig. 4.1). The overall increase in A_T is partly a consequence of increasing salinities in the Nordic Seas in the past decades (Fig. S2, S19), which also have been observed in many studies and has been explained to be a result of changes in the inflowing Atlantic Water related to subpolar gyre strength (Holliday et al., 2008; Lauvset et al., 2018). The increasing salt content does not only affect A_T, but also equally C_T. This effect is, however, about the same magnitude as the A_T driver, but in opposite direction (Fig. S19). The effect of changes in temperature on pH in the surface layer is relatively small. In contrast to several studies pointing towards a warming of the Nordic Seas (e.g. Holliday et al.,

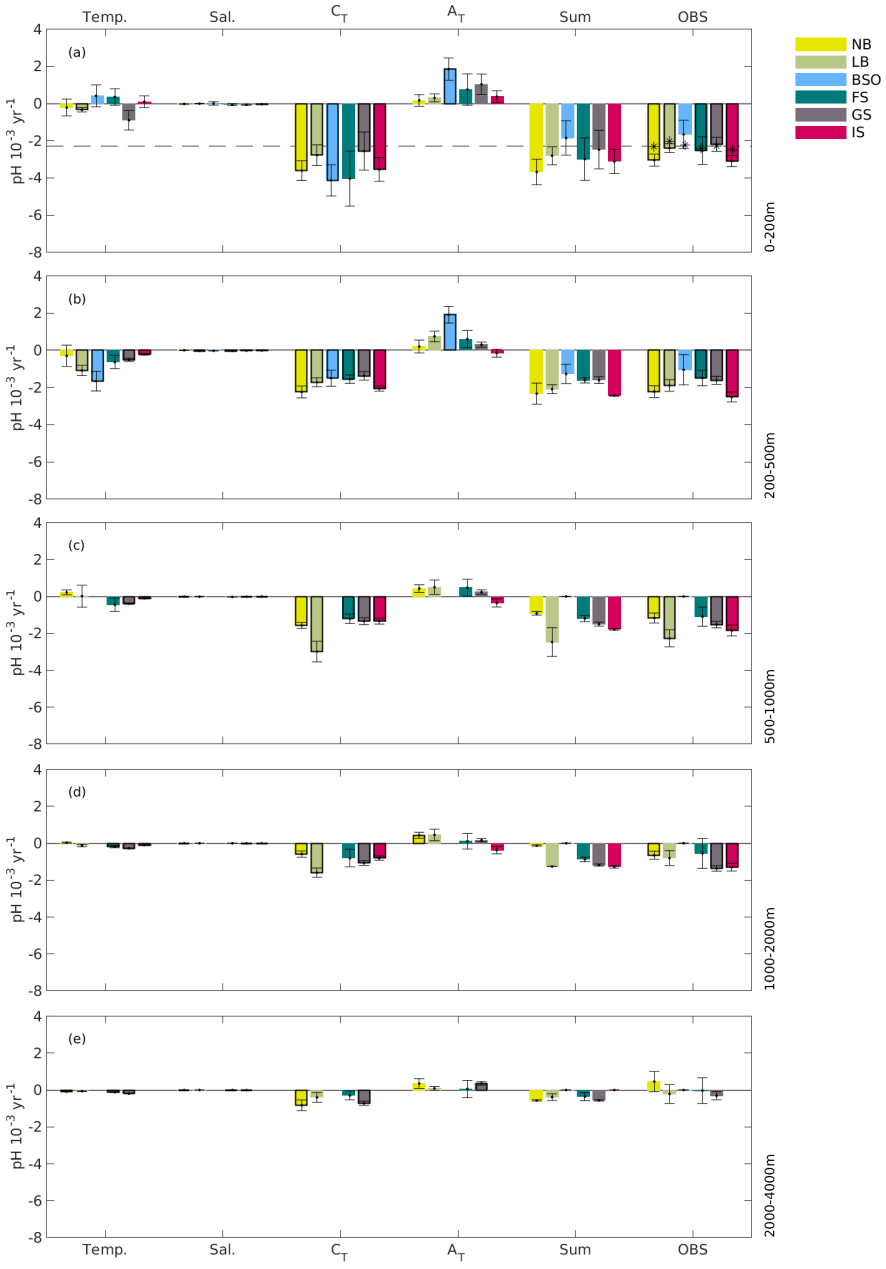

Figure 11. Contribution of observed changes in temperature, salinity, C_T, A_T to the observed trend in pH (OBS) over the 1981-2019 period. Bars showing trends that are significantly different from zero are outlined with a black line. Sum indicates the total trend in pH calculated as the sum of the trends associated with these four driving factors. The dashed line and black asterisks indicate the pH trends expected from the change in atmospheric CO_2 during the same period for the whole area and for the separate basins, respectively.

2008; Blindheim and Østerhus, 2013; Lauvset et al., 2018; Ruiz-Barradas et al., 2018), the Barents Sea Opening, the Eastern Fram Strait and the Iceland Sea here show a tendency, although insignificant, towards a cooling, which slightly increases pH. The ambiguous effect of temperature in surface waters is a result of unequal distribution of sampling over the seasons. When calculating trends with all available temperature data, not only the ones that accompanied the C_T and A_T data, we obtain a clear warming signal (not shown). In an attempt to estimate the effect of seasonal under sampling on our surface pH trends, we also calculated the trends and their drivers by using data from the productive season (April-September) only. The pH trends obtained from these data are not significantly different from the ones in Fig. . However, the trend in the Barents Sea Opening is now of similar size as in the other regions. The temperature has now a reinforcing effect on the pH decline. This suggest that the weak apparent trend in pH in Fig. is a result of a seasonal undersampling of temperature.

In deeper layers, there is an overall increase in C_T, A_T (except in the Iceland Sea), salinity, and temperature. Although the effect of increasing C_T is reduced away from the surface as a consequence of the gradual isolation of deeper waters from the atmosphere, it remains the main driver of pH change down to 2000 m, with a few exceptions. In the 200-500 m layer in the Lofoten Basin and the Barents Sea Opening, there is an increase in temperature, leading to a pH decline that is almost as large as that from the C_T increase. In the Barents Sea Opening, the increase of A_T in the 200-500 m layer is as large as in the surface layer, and in the 1000-2000 m layer in the Norwegian Basin, there is an increase in A_T that almost cancels the effect of increasing C_T. Below 2000 m, the effects of changes in A_T are of similar size as the effect of changes in C_T in all basins. As for the surface layer, part of the C_T and A_T increase can be explained by increasing salinites, but there is also a biogeochemical component (Fig. S19). The uncertainties in the freshwater and biogeochemical components are, however, large, making the decomposition uncertain. The warming seen in the deep waters is likely a result of the decreased deep-water formation in the Greenland Sea and the following increased exchange with warmer Arctic deep waters (e.g. Østerhus and Gammelsrød, 1999; Blindheim and Rey, 2004; Karstensen et al., 2005; Somavilla et al., 2013). The relatively strong trends in C_T and pH in the upper 2000m of the Greenland and Iceland seas could be a consequence of deep winter mixing (Våge et al., 2015; Brakstad et al., 2019). However, the convection in the Iceland Sea has only been documented to reach depths of 200-400 m (Ólafsson, 2003; Våge et al., 2015). The signal in the deep Iceland Sea is therefore likely a result of spreading of intermediate waters from the Greenland Sea (Messias et al., 2008; Jeansson et al., 2017). Also in the Norwegian Basin there is a significant trend down to 2000 m, although weaker than in the other basins. This is likely also a result of advection from the Greenland Sea (Blindheim, 1990; Blindheim and Rey, 2004; Jeansson et al., 2017). The strong trends in C_T in the Lofoten Basin could be a result of a combination of the persistent eddy in this area (dominating the upper 1000 m), and advection of intermediate water from the Greenland Sea at about 1000-1500 m (Jeansson et al., 2017).

The water-masses in the 2000-4000 m range are increasingly dominated by old Arctic deep waters (e.g. Somavilla et al., 2013). With ages of around or more than 200 years (Jutterström and Jeansson, 2008; Stöven et al., 2016), they have been isolated from the increasing anthropogenic CO_2, which explains the weak trends at these depths.

The exceptionally strong trends in A_T in the surface and the 200-500 m layer in Barents Sea Opening are intriguing. Considering that the strong A_T trend also exists in the 200-500 m layer, it is likely not a result of seasonal undersampling. Further, the salinity decomposition in Fig. S19 in the Supplementary material suggest that it is not a result of changing salinity, but rather of

biogeochemical processes. While this decomposition gives clear results in the 200-500 m layer, the uncertainty of the freshwater component is as large as the biogeochemical component in the surface layer, making the decomposition, and therefore the role of changes in freshwater content and biogeochemical processes, uncertain. This is a result of the uncertainty in the salinity trend (Fig. S2), which could be caused by the presence of the relatively fresh, Norwegian Coastal Current that has been shown to occasionally, under specific wind conditions, spread into the Barents Sea Opening Olsen et al. (2003). One biogeochemical process that could have a potential impact the Barents Sea A_T trend is the recurrent blooms of calcifying coccolithophorids (Giraudeau et al., 2016), which consumes A_T during growth, and releases A_T when their shells are decomposed. There is an indication of an increase in their presence in the Barents Sea (Giraudeau et al., 2016; Oziel et al., 2020). In which direction this would impact the A_T depends on horizontal advection, remineralization and burial, and deserves separate dedicated process studies.

For past and future changes, the drivers of surface pH change show similar spatial patterns, except for temperature (Fig. 12). As for the present day changes, the main driver of pH change is an increase in C_T, which is larger in Atlantic Water than in polar waters. The larger increase in C_T in the Atlantic Water, which is in agreement with what has been observed over the last 2-3 decades (Olsen et al., 2006), can partly be related to their higher buffer capacity (Sect. 1.1). In polar waters, C_T is additionally diluted by the increased freshwater export from the Arctic Ocean (Shu et al., 2018) that to varying degree counteracts the effect of atmospheric CO_2 uptake. The increasing freshwater export also results in a dilution of A_T and salinity in polar waters that have, respectively, a negative and positive contribution to the pH trend. While the effect of A_T dilution is on the same order of magnitude as the effect of C_T dilution, the effect of the reduction in salinity is minor. The Atlantic Waters show a tendency towards increasing A_T and salinity that partly reduces/amplify the decrease in pH. The temperature has an overall negative effect on the pH trend as a result of an overall warming. From past to present, present to future RCP2.6, the temperature increase is almost non-existing in polar waters, indicating that it has been shielded from warming through the presence of sea ice. In some smaller regions there is even a sign of a cooling, which could be a result of an increased presence of polar waters due to the increasing freshwater export.

The combined effect of these drivers explain the zonal gradients in the pH decrease that we saw in Sect. 3.2 and 3.4. From past to present, the largest pH decrease take place in the Atlantic Water due to a stronger uptake of anthropogenic carbon and a stronger warming in these waters. The increasing freshwater export from the Arctic, and the dilution of A_T, plays an important role in the eastern Nordic Seas, but it does not override the acidification rate in the Atlantic Water. From present-future, the freshwater export and dilution of A_T plays a bigger role, and the acidification becomes larger in polar waters compared to Atlantic Water. For the changes from past-present, and present to future RCP2.6, the zonal gradient in Ω_{Ar} drops follows that of pH, showing the importance of the competing effect of A_T dilution in polar waters, and C_T uptake in Atlantic Water, respectively. In RCP8.5, there is, in contrast to pH, a larger drop in the easter part. This can be explained by the larger changes in temperature, which affects Ω_{Ar} in the opposite direction.

In the historical run and all three future projections of NorESM1-ME, the change in surface ocean pCO_2 differs from the change in the atmosphere (Fig. S14). From past to present, there is an increase in the undersaturation, i.e. the positive trend in the oceanic pCO_2 lags the trend in the atmosphere. This means that the pH decrease is less than that expected from the increase in

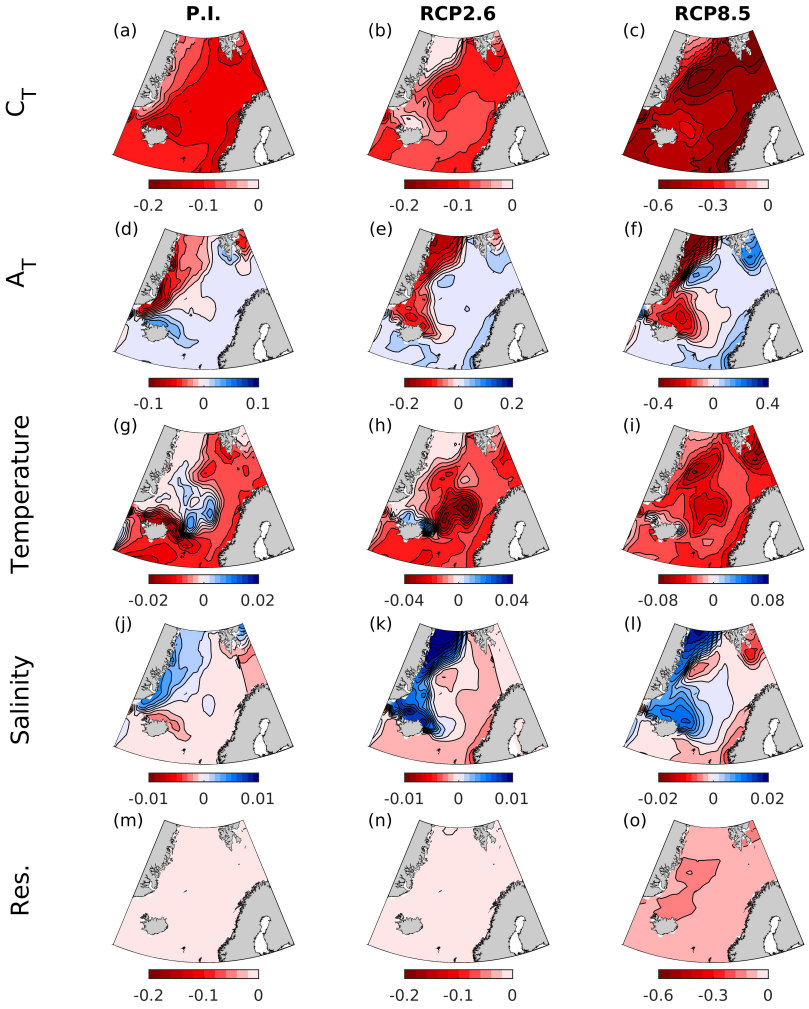

Figure 12. Contribution of modelled changes in surface C_T, A_T, temperature, and salinity, to the change in pH between 1850-1859 and 1996-2005 (P.I.), and 1996-2005 and 2090-2099 (RCP2.6 and RCP8.5). Res. shows the residual between the total change in pH, calculated as the sum of the trends associated with these four driving factors, and the actual change shown in Figs. 4,8,10.

atmospheric CO_2. The lag continues into all the future scenarios, but from around 2040 and onward the oceanic pCO_2 increases faster than that of the atmosphere, resulting in a decreasing undersaturation. In RCP2.6 and 4.5 this gives rise to, on average, stronger decreases in pH (from 1996-2005 to 2090-2099) than expected from the rise in atmospheric CO_2. In RCP8.5, however, the difference between the end-of-the century ocean and atmospheric pCO_2 is still larger than the present day, meaning that

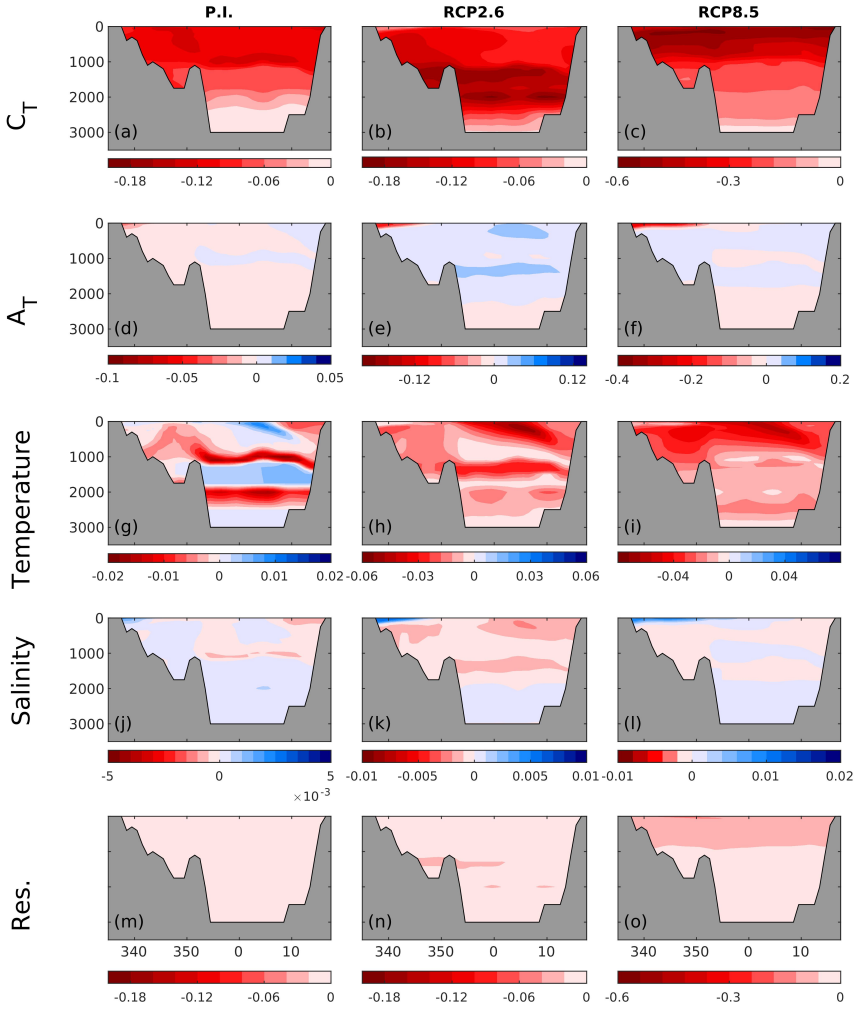

Figure 13. Contribution of modelled changes in surface temperature, salinity, C_T, A_T to the change in pH between 1850-1859 and 1996-2005 (P.I.), and 1996-2005 and 2090-2099 (RCP2.6 and RCP8.5) at the depth section at 70°N. Res. shows the residual between the total change in pH, calculated as the sum of the trends associated with these four driving factors, and the actual change shown in Figs. 5,9.

the decrease in pH is less than expected. As detailed above there are several mechanisms underlying undersaturation of surface ocean pCO_2 in the Nordic Seas, but further analyses of these, including their potential future changes, is beyond the scope of this paper.

Below the surface layer, C_T is also the main driver of past and future pH changes (Fig. 13). The change from pre-industrial to present indicates a gradually weaker impact of C_T with depth, except for a tongue at about 1000 m depth that connects to the surface in the Iceland sea. This is most likely related to the deep water formation in this region that spreads at depth. The end-of-the-century C_T increase under the RCP2.6 scenario is larger in the deep than in the surface layer, resulting in the stronger pH reduction at mid-depths as seen in Fig. 9. This mid-depth layer with a strong acidification is partly a result of the higher atmospheric CO_2 concentrations in the middle of the 21st century , in combination with the rapid ventilation of the water column in this area, i.e. when these waters were at surface they were exposed to peak atmospheric CO_2. However, the large C_T increase in deep waters is also partly explained by increased remineralization, as indicated by a $\sim$1 ml O_2 l^{-1} increase in the apparent oxygen utilization (AOU) at depths of 1800-2100 m in both RCP2.6 and RCP8.5 (not shown) throughout the Nordic Seas. Assuming Redfield (O_2:C=132:106) this corresponds to a change in C_T of $\sim$30 μmol kg^{-1}, which results to a pH decrease of $\sim$0.1 at the alkalinity in question. Impacts of changes in A_T, salinity and temperature, are relatively modest at depth.

The residual between the sum of the four drivers and the actual pH change (Figs. 12 and 13) can be attributed to approximations involved in the decomposition, including the assumption of a linear trend and the use of temporal means (Takahashi et al., 1993; Lenton et al., 2012; Lauvset et al., 2015). These assumptions are least appropriate for the RCP8.5 scenario, where the changes are largest, and therefore the residual is especially large for this scenario. Although the absolute numbers related to the drivers should be taken with care, this decomposition still gives a good estimate of the relative importance of temperature, salinity, C_T, and A_T on pH changes.

4.2 Implications for cold-water corals

Cold-water corals build their structures out of aragonite, which is the more soluble form of calcium carbonate. To some degree, living corals can compensate for aragonite undersaturation in seawater and increase their internal pH by 0.3-0.6 (McCulloch et al., 2012; Allison et al., 2014). For some time these corals can therefore continue to calcify in waters with Ω_{Ar}<1, however, the calcification rates and breaking strength of the structures of the most abundant coral organism, *Lophelia pertusa*, is reduced under such conditions (Hennige et al., 2015). Furthermore, dead coral structures, which compose a major part of the reefs, cannot resist corrosive waters and experience increased dissolution rates in a situation with Ω_{Ar}<1. Cold-water coral reefs, along with their ecosystems, are therefore likely to collapse if the water they live in becomes undersaturated in aragonite. It has been estimated that globally about 70% of the deep sea corals will be below the aragonite saturation horizon by the end-of-the-century under high-emission-scenarios (Guinotte et al., 2006; Zheng and Cao, 2014).

Most of the reef sites that have been identified in the Nordic Seas (321 out of the 324 within the region defined in Fig. 1) are at depths of 0-500 m (Fig. 14, see also Buhl-Mortensen et al. (2015)). The current aragonite saturation horizon is at 2000 m, with uncertainty range 1750-2500 m. Note that the uncertainty range of the depth of the saturation horizon is not equally distributed around the mean because the uncertainty analysis is done for the saturation state, from which the depth distribution is calculated. From observations we also see that the waters in the depth range 1000-2000 m are close to being undersaturated in aragonite (Sect. 3.3). In the emission-driven RCP2.6 scenario, NorESM1-ME projects that the aragonite

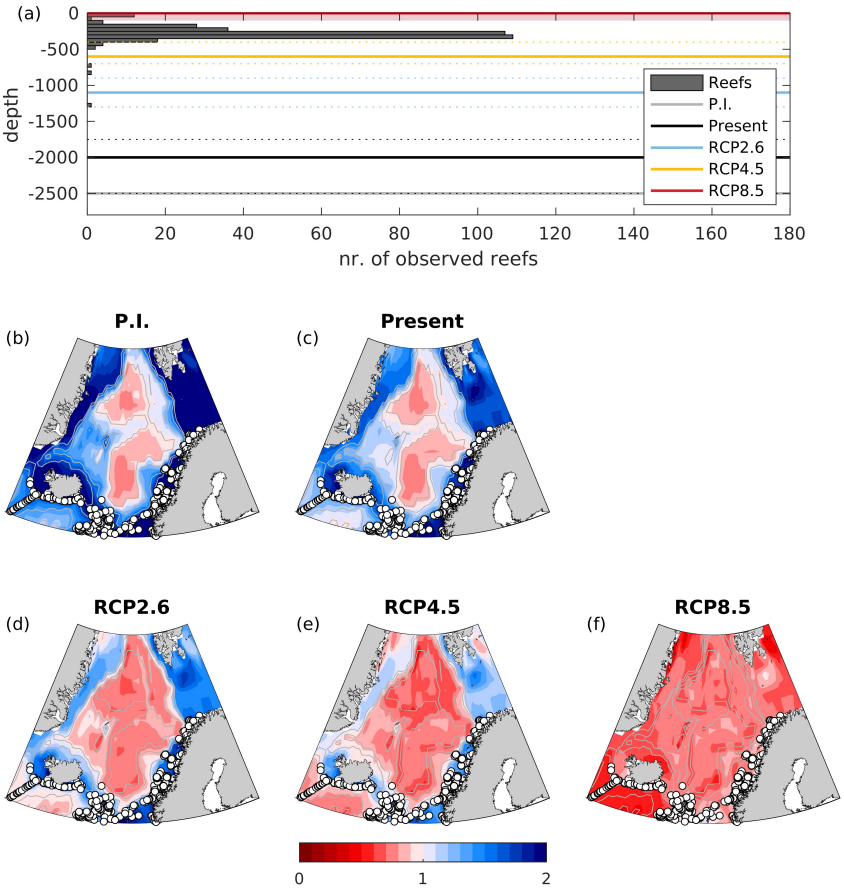

Figure 14. Number of observed reef sites per 50 m depth interval together with the aragonite saturation horizons (solid lines) in the Nordic Seas for past (1850-1879), present (1980-2005) and future (2070-2099) under the emission-driven RCP2.6, RCP4.5 and RCP8.5 scenarios calculated from the GLODAPv2 climatology and NorESM1-ME simulations. The dashed lines show the uncertainty (σ_2). The red shading shows the projection uncertainty as estimated from our ESM ensemble for RCP8.5. (a) and maps showing aragonite saturation state of bottom waters (calculated from the GLODAPv2 climatology and NorESM1-ME simulations) together with positions of observed reefs (b-f).

saturation horizon will shoal to 1100 m (uncertainty: 900-1300 m) by the end of the century. In the emission-driven RCP4.5 scenario, the saturation horizon is projected to shoal to 600 m depth (uncertainty: 400-800 m) by the end of this century. This implies that the deepest observed reefs will be exposed to corrosive waters, and thus experience elevated costs of calcification and dissolution of dead structures. The majority (315 out of 324) of the coral sites in the Nordic Seas are, however, found at shallower depths than the projected saturation horizon with its uncertainty, although the margins are small. Also García-Ibáñez et al. (2021) suggested that cold-water corals in the subpolar North Atlantic will be exposed to corrosive waters if the 2-degree goal (which is the aim of RCP2.6) is not met. In the RCP8.5 scenario, NorESM1-ME projects the whole water column to be

undersaturated in aragonite at the end of this century, such that all cold-water coral reefs in the Nordic Seas will be exposed to corrosive waters. Because of the low Ω_{Ar} in surface waters, the uncertainty of Ω_{Ar} related to mapping, measurements and dissociation constants does not result in any uncertainty in the saturation horizon in this scenario (i.e. $\Omega_{Ar} < 1$ in the surface waters also when taking into account the uncertainties). For RCP8.5 the NorESM1-ME results are consistent with our CMIP5 model ensemble that suggests that the future saturation horizon lies in the range of 0 and 100 m. Comparison with the CMIP5 ensemble is not possible for RCP2.6 and RCP4.5 because few of the models have performed emission-driven runs under these scenarios. However, NorESM1-ME simulates among the stronger drops in pH in all depth layers considered in Fig. S5, and have also been shown be in the upper end of absorption of anthropogenic carbon in the Arctic Ocean (Terhaar et al., 2020a), suggesting that out estimates of the future saturation horizon lies in the upper bound of possible future states.

5 Summary and Conclusions

We have provided a detailed analysis of spatial and temporal variations of past, present and future acidification, and its drivers, in the Nordic Seas. We have further assessed the potential impacts of this acidification on aragonite saturation and cold-water coral reefs.

pH changes and its potential ecosystem impacts

From 1850 to 1980 both the model simulation of NorESM1-ME and observational data, together with the GLODAPv2 pre-industrial estimate, suggest that the pH of Nordic Seas surface waters has dropped by 0.06, which is similar to the pH decrease of the global surface ocean. During this period, the aragonite saturation horizon has slightly shallowed, but has remained well below the depths of known cold-water coral habitats. During the last 39 years covered by this study, when regular sampling of carbon system variables have been made in the region, the pH of the Nordic Seas surface waters has decreased at a rate of -2.79$\pm$0.3 10^{-3} yr^{-1} on average, resulting in a pH decline of 0.11 between 1981 and 2019. This decrease is stronger than the decrease observed for the global ocean of -1.80$\pm$0.4 10^{-3} yr^{-1} for the period 1991-2011 (Lauvset et al., 2015). The pH reductions are significant all over the Nordic Seas surface waters, except in the Barents Sea Opening. In some regions the acidification is detectable down to 2000 m, which we attribute to the deep water formation an how these water-masses spreads at depth, and the waters at 1000-2000 m throughout the Nordic Seas have approached aragonite undersaturation. An additional pH drop of 0.1-0.4 in the surface waters is projected until the end of the century, depending on the emission scenario. In the high-emission scenario, RCP8.5, all cold-water coral reefs will be exposed to corrosive waters by the end of the 21st century, threatening not only their existence, but also that of their associated ecosystems. This is confirmed by an CMIP5-ensemble of 7 models, whose members all agree on these consequences. The NorESM1-ME simulations suggest that some cold-water corals will be exposed to undersaturation also under the RCP4.5 scenario, and that this only can be avoided by keeping the emissions within the limits prescribed in the RCP2.6 scenario. In comparison to our ESM-ensemble, NorESM1-ME tends to simulate shallow saturation horizons. These results can therefore be considered as careful estimates.

pH drivers

The acidification during the last 39 years is mainly driven by increasing C_T coming from the uptake of anthropogenic carbon. The effects of increasing C_T is slightly opposed by increasing A_T, which partly comes as a result of the increasing salinities, i.e. "the salinification", of the Nordic Seas. While in the deep waters there is a clear warming signal, which has contributed to the decreasing pH, the impact of temperature in the surface is ambiguous, and even shows a cooling in some places. We find this apparent cooling to be a result seasonal undersampling, which further complicates a comparison of the changes in sea surface pCO_2 to the atmospheric one. In the Barents Sea Opening, there is an exceptionally strong increase in A_T, which we cannot relate to increasing salinity. The reasons behind this strong increase is then either a result of biogeochemical processes, or can also be a result sampling issues. Unfortunately, we cannot pin this down with the dataset we have, and this remains as an open question for future investigations.

Also for past and future changes, increasing C_T is the main driver of pH change in the Nordic Seas, but here we can distinguish some regional differences related to the different water-masses. In the Atlantic Water, the pH change is mainly driven by increasing C_T and temperatures, and slightly opposed by increasing A_T related to a salinification, as we also see in our observational dataset for the period of 1981-2019. In polar waters, however, there is a clear signal of increasing freshwater export from the Arctic which has an important impact on the acidification through dilution of C_T, A_T, and salinity. The dilution of C_T slightly opposes the effect of uptake of anthropogenic carbon, which increases the relative impact of decreasing A_T on the pH drop. The absence of this freshwater signal in our observational dataset might be a result of the relatively short time scale, but it is also possible that our regions are located to far to the East.

Data availability. The GLODAPv2.2019 data and GLODAPv2 mapped climatologies are available for download at https://www.glodap.info/index.php/merged-and-adjusted-data-product-v2-2019/ and https://www.glodap.info/index.php/mapped-data-product/ , respectively.

The data from Ocean Weather station M from 2001-2007 is available in GLODAPv2.2019. Data from the time period 2008-2019 will be available in the next GLODAP version.

The data from the time-series station in the Iceland Sea can be obtained from the NCEI database (Ólafsson, 2012; Ólafsdóttir et al., 2020)

The data from the Norwegian ocean acidification monitoring program (Chierici et al., 2019a), and from the Eastern Fram Strait (Chierici and Fransson, 2019) is available at the Norwegian Marine Data Centre (NMDC).

The ESM simulations can be downloaded at https://esgf-node.llnl.gov/search/cmip5/

The cold-water coral positions have been derived from data that is made available under the European Marine Observation Data Network (EMODnet) Seabed Habitats initiative (www.emodnet-seabedhabitats.eu), financed by the European Union under Regulation (EU) No 508/2014 of the European Parliament and of the Council of 15 May 2014 on the European Maritime and Fisheries Fund.

Author contributions. AO, FF and FF designed the research. FF, FF, and AO performed the data-analysis with inputs from NG, IS, MC and EJ. FF lead the writing of the manuscript with inputs from all co-authors. JT designed, tested, and performed the NorESM1-ME model simulations.

Competing interests. The authors declare that they have no conflict of interest.

Disclaimer. TEXT

Acknowledgements. F. Fransner was funded by the Bjerknes Centre for Climate Research and by the Research Council of Norway through the project The Nansen Legacy (RCN 276730). F. Fröb was funded by the Bjerknes Centre for Climate Research. JT acknowledges funding from Research Council of Norway (Reef-Futures no. 295349 and Columbia no. 275268). NG acknowledges funding from the Research Council of Norway (IMPOSE, 294930). SKL acknowledges funding from the Research Council of Norway (NorArgo2, 269753) High-performance computing and storage resources were provided by the Norwegian infrastructure for computational science (through projects nn1002k and ns1002k). The Norwegian Ocean Acidification Monitoring Program is funded by the Norwegian Environmental Agency through project no. 17078007. The flagship program" Monitoring ocean acidification in Norwegian waters" within the FRAM-High North Research Centre for Climate and the Environment. We acknowledge the World Climate Research Programme's Working Group on Coupled Modelling, which is responsible for CMIP, and we thank the climate modeling groups for producing and making available their model output. For CMIP, the U.S. Department of Energy's Program for Climate Model Diagnosis and Intercomparison provides coordinating support and led development of software infrastructure in partnership with the Global Organization for Earth System Science Portals.

References

Allison, N., Cohen, I., Finch, A., Erez, J., and Tudhope, A.: Corals concentrate dissolved inorganic carbon to facilitate calcification, Nature Communications, 5, https://doi.org/doi:10.1038/ncomms6741, 2014.

Anderson, L. G.: Dissolved inorganic carbon, pH, alkalinity, temperature, salinity and other variables collected from discrete sample and profile observations using CTD, bottle and other instruments from the LANCE in the Barents Sea from 1986-07-19 to 1986-07-26 (NCEI Accession 0113910). NOAA National Centers for Environmental Information. Dataset., https://doi.org/10.3334/cdiac/otg.carina$_5$8la19860719, $dataset$, 2013a.

Anderson, L. G.: Dissolved inorganic carbon, pH, alkalinity, temperature, salinity and other variables collected from discrete sample and profile observations using CTD, bottle and other instruments from the ODEN in the Arctic Ocean, Barents Sea and others from 2002-04-20 to 2002-06-06 (NCEI Accession 0113590). NOAA National Centers for Environmental Information., https://doi.org/10.3334/cdiac/otg.carina$_7$7dn20020420, $dataset$, 2013b.

Anderson, L. G. and Olsen, A.: Air–sea flux of anthropogenic carbon dioxide in the North Atlantic, Geophysical Research Letters, 29, 16–1–16–4, https://doi.org/10.1029/2002GL014820, https://agupubs.onlinelibrary.wiley.com/doi/abs/10.1029/2002GL014820, 2002.

Anderson, L. G., Blindheim, J., and Rey, F.: Dissolved inorganic carbon, pH, alkalinity, temperature, salinity and other variables collected from discrete sample and profile observations using CTD, bottle and other instruments from the JOHAN HJORT in the North Greenland Sea and Norwegian Sea from 1997-04-14 to 1997-05-22 (NCEI Accession 0113563). NOAA National Centers for Environmental Information., https://doi.org/10.3334/cdiac/otg.carina$_5$8jh19970414, $dataset$, 2013a.

Anderson, L. G., Johannessen, T., and Rey, F.: Dissolved inorganic carbon, pH, alkalinity, temperature, salinity and other variables collected from discrete sample and profile observations using CTD, bottle and other instruments from the JOHAN HJORT in the North Greenland Sea and Norwegian Sea from 1998-08-01 to 1998-08-23 (NCEI Accession 0113758). NOAA National Centers for Environmental Information., https://doi.org/10.3334/cdiac/otg.carina$_5$8jh19980801, $dataset$, 2013b.

Arora, V. K., Scinocca, J. F., Boer, G. J., Christian, J. R., Denman, K. L., Flato, G. M., Kharin, V. V., Lee, W. G., and Merryfield, W. J.: Carbon emission limits required to satisfy future representative concentration pathways of greenhouse gases, Geophysical Research Letters, 38, https://doi.org/https://doi.org/10.1029/2010GL046270, https://agupubs.onlinelibrary.wiley.com/doi/abs/10.1029/2010GL046270, 2011.

Bellerby, R. G. J. and Smethie, William M., J.: Dissolved inorganic carbon, alkalinity, temperature, salinity and other variables collected from discrete sample and profile observations using CTD, bottle and other instruments from the KNORR in the Barents Sea, North Atlantic Ocean and others from 2002-05-30 to 2002-07-01 (NCEI Accession 0113569). NOAA National Centers for Environmental Information., https://doi.org/10.3334/cdiac/otg.carina$_3$16n20020530, $dataset$, 2013.

Bellerby, R. G. J., Olsen, A., Furevik, T., and Anderson, L. G.: Response of the Surface Ocean CO2 System in the Nordic Seas and Northern North Atlantic to Climate Change, pp. 189–197, American Geophysical Union (AGU), https://doi.org/https://doi.org/10.1029/158GM13, https://agupubs.onlinelibrary.wiley.com/doi/abs/10.1029/158GM13, 2005.

Bentsen, M., Bethke, I., Debernard, J. B., Iversen, T., Kirkevåg, A., Seland, Ø., Drange, H., Roelandt, C., Seierstad, I. A., Hoose, C., and Kristjánsson, J. E.: The Norwegian Earth System Model, NorESM1-M – Part 1: Description and basic evaluation of the physical climate, Geoscientific Model Development, 6, 687–720, https://doi.org/10.5194/gmd-6-687-2013, https://gmd.copernicus.org/articles/6/687/2013/, 2013.

Bleck, R. and Smith, L. T.: A wind-driven isopycnic coordinate model of the north and equatorial Atlantic Ocean: 1. Model development and supporting experiments, Journal of Geophysical Research: Oceans, 95, 3273–3285, https://doi.org/10.1029/JC095iC03p03273, https://agupubs.onlinelibrary.wiley.com/doi/abs/10.1029/JC095iC03p03273, 1990.

Blindheim, J.: Arctic intermediate water in the Norwegian sea, Deep Sea Research Part A. Oceanographic Research Papers, 37, 1475 – 1489, https://doi.org/https://doi.org/10.1016/0198-0149(90)90138-L, http://www.sciencedirect.com/science/article/pii/019801499090138L, 1990.

Blindheim, J. and Østerhus, S.: The Nordic Seas, Main Oceanographic Features, pp. 11–37, American Geophysical Union (AGU), https://doi.org/10.1029/158GM03, https://agupubs.onlinelibrary.wiley.com/doi/abs/10.1029/158GM03, 2013.

Blindheim, J. and Rey, F.: Water-mass formation and distribution in the Nordic Seas during the 1990s, ICES Journal of Marine Science, 61, 846–863, https://doi.org/10.1016/j.icesjms.2004.05.003, https://doi.org/10.1016/j.icesjms.2004.05.003, 2004.

Bockmon, E. E. and Dickson, A. G.: An inter-laboratory comparison assessing the quality of seawater carbon dioxide measurements, Marine Chemistry, 171, 36–43, https://doi.org/https://doi.org/10.1016/j.marchem.2015.02.002, https://www.sciencedirect.com/science/article/pii/S0304420315000213, 2015.

Booth, B. B. B., Bernie, D., McNeall, D., Hawkins, E., Caesar, J., Boulton, C., Friedlingstein, P., and Sexton, D. M. H.: Scenario and modelling uncertainty in global mean temperature change derived from emission-driven global climate models, Earth System Dynamics, 4, 95–108, https://doi.org/10.5194/esd-4-95-2013, https://esd.copernicus.org/articles/4/95/2013/, 2013.

Bopp, L., Resplandy, L., Orr, J. C., Doney, S. C., Dunne, J. P., Gehlen, M., Halloran, P., Heinze, C., Ilyina, T., Séférian, R., Tjiputra, J., and Vichi, M.: Multiple stressors of ocean ecosystems in the 21st century: projections with CMIP5 models, Biogeosciences, 10, 6225–6245, https://doi.org/10.5194/bg-10-6225-2013, https://bg.copernicus.org/articles/10/6225/2013/, 2013.

Brakstad, A., Våge, K., Håvik, L., and Moore, G. W. K.: Water Mass Transformation in the Greenland Sea during the Period 1986–2016, Journal of Physical Oceanography, 49, 121–140, https://doi.org/10.1175/JPO-D-17-0273.1, https://doi.org/10.1175/JPO-D-17-0273.1, 2019.

Brewer, P. G., Takahashi, T., and Williams, R. T.: Partial pressure (or fugacity) of carbon dioxide, dissolved inorganic carbon (DIC), total alkalinity, water temperature, salinity, dissolved oxygen concentration and other variables collected from discrete sample and profile observations during R/V Knorr TTO-NAS cruises in the North Atlantic Ocean from 1981-04-01 to 1981-10-19 (NCEI Accession 0000733). NOAA National Centers for Environmental Information., https://doi.org/10.3334/cdiac/otg.ndp004, dataset, 2010.

Buhl-Mortensen, L., Olafsdottir, S. H., Buhl-Mortensen, P., Burgos, J. M., and Ragnarsson, S. A.: Distribution of nine cold-water coral species (Scleractinia and Gorgonacea) in the cold temperate North Atlantic: effects of bathymetry and hydrography, Hydrobiologia, 759, 39–61, https://doi.org/10.1007/s10750-014-2116-x, https://doi.org/10.1007/s10750-014-2116-x, 2015.

Caldeira, K. and Wickett, M. E.: Anthropogenic carbon and ocean pH, Nature, 425, 365–365, https://doi.org/10.1038/425365a, https://doi.org/10.1038/425365a, 2003.

Chafik, L. and Rossby, T.: Volume, Heat, and Freshwater Divergences in the Subpolar North Atlantic Suggest the Nordic Seas as Key to the State of the Meridional Overturning Circulation, Geophysical Research Letters, 46, 4799–4808, https://doi.org/10.1029/2019GL082110, https://agupubs.onlinelibrary.wiley.com/doi/abs/10.1029/2019GL082110, 2019.

Chierici, M. and Fransson, A.: Seasonal variability of the marine CO_2 system and nutrients in the Atlantic water inflow to the Arctic Ocean in 2014, https://doi.org/10.21335/NMDC-154415697, dataset, 2019.

Chierici, M., Sørensen, K., Johannessen, T., Børsheim, K., A.Olsen, Yakushev, E., Omar, A., and Blakseth, T.: Tillførselprogrammet 2011, Overvåking av havsforsuring av norske farvann. Rapport, Klif, TA2936-2012, Tech. rep., 2012.

Chierici, M., Sørensen, K., Johannessen, T., Børsheim, K., A.Olsen, Yakushev, E., Omar, A., Skjelvan, I., Norli, M., , and Lauvset, S.: Tillførselprogrammet 2012, Overvåking av havsforsuring av norske farvann. Rapport, Klif, TA3043-2013, Tech. rep., 2013.

Chierici, M., Skjelvan, I., Bellerby, R., M. Norli, L. F., Hodal, H., Børsheim, K., Lauvset, S., Johannessen, T., Sørensen, K., and Yakushev, E.: Overvåking av havforsuring av norske farvann. Rapport, Miljødirektoratet M-218, Tech. rep., 2014.

Chierici, M., Skjelvan, I., Norli, M., Lødemel, H., Lunde, L., Sørensen, K., Yakushev, E., Bellerby, R., King, A., Lauvset, S., Johannessen, T., and Børsheim, K.: Overvåking av havforsuring i norske farvann i 2014, Rapport, Miljødirektoratet, M-354, Tech. rep., 2015.

Chierici, M., Skjelvan, I., Norli, M., Børsheim, K., Lauvset, S., Lødemel, H., Sørensen, K., King, A., Kutti, T., Renner, A., Omar, A., and Johannessen, T.: Overvåking av havforsuring i norske farvann i 2015, Rapport, Miljødirektoratet, M-573, Tech. rep., 2016.

Chierici, M., Skjelvan, I., Norli, M., Jones, E., Børsheim, K., Lauvset, S., Lødemel, H., Sørensen, K., King, A., and Johannessen, T.: Overvåking av havforsuring i norske farvann i 2016, Rapport, Miljødirektoratet, M-776, Tech. rep., 2017.

Chierici, M., Jones, E., and Lødemel, H. H.: Interannual variability of the marine CO_2 system and nutrients in the Norwegian Sea from 2011 to 2017, https://doi.org/10.21335/NMDC-1939716216, dataset, 2019a.

Chierici, M., Vernet, M., Fransson, A., and Børsheim, K. Y.: Net Community Production and Carbon Exchange From Winter to Summer in the Atlantic Water Inflow to the Arctic Ocean, Frontiers in Marine Science, 6, 528, https://doi.org/10.3389/fmars.2019.00528, https://www.frontiersin.org/article/10.3389/fmars.2019.00528, 2019b.

Dai, A., Luo, D., Song, M., and Liu, J.: Arctic amplification is caused by sea-ice loss under increasing CO2, Nature Communications, 10, 121, https://doi.org/10.1038/s41467-018-07954-9, https://doi.org/10.1038/s41467-018-07954-9, 2019.

Dickson, A., Sabine, C., and Christian, J. e.: Guide to best practices for ocean CO2 measurement., PICES Special Publication 3; IOCCP Report 8, 2007.

Dickson, A. G.: Standard potential of the reaction: AgCl(s) + 12H2(g) = Ag(s) + HCl(aq), and and the standard acidity constant of the ion HSO4- in synthetic sea water from 273.15 to 318.15 K, The Journal of Chemical Thermodynamics, 22, 113 – 127, https://doi.org/https://doi.org/10.1016/0021-9614(90)90074-Z, http://www.sciencedirect.com/science/article/pii/002196149090074Z, 1990.

Dickson, R. R. and Brown, J.: The production of North Atlantic Deep Water: Sources, rates, and pathways, Journal of Geophysical Research: Oceans, 99, 12 319–12 341, https://doi.org/10.1029/94JC00530, https://agupubs.onlinelibrary.wiley.com/doi/abs/10.1029/94JC00530, 1994.

Doney, S. C., Fabry, V. J., Feely, R. A., and Kleypas, J. A.: Ocean Acidification: The Other CO_2 Problem, Annual Review of Marine Science, 1, 169–192, https://doi.org/10.1146/annurev.marine.010908.163834, https://doi.org/10.1146/annurev.marine.010908.163834, pMID: 21141034, 2009.

Doney, S. C., Busch, D. S., Cooley, S. R., and Kroeker, K. J.: The Impacts of Ocean Acidification on Marine Ecosystems and Reliant Human Communities, Annual Review of Environment and Resources, 45, null, https://doi.org/10.1146/annurev-environ-012320-083019, https://doi.org/10.1146/annurev-environ-012320-083019, 2020.

Doo, S. S., Kealoha, A., Andersson, A., Cohen, A. L., Hicks, T. L., Johnson, Z. I., Long, M. H., McElhany, P., Mollica, N., Shamberger, K. E. F., Silbiger, N. J., Takeshita, Y., and Busch, D. S.: The challenges of detecting and attributing ocean acidification impacts on marine ecosystems, ICES Journal of Marine Science, https://doi.org/10.1093/icesjms/fsaa094, https://doi.org/10.1093/icesjms/fsaa094, fsaa094, 2020.

Dufresne, J.-L., Foujols, M.-A., Denvil, S., Caubel, A., Marti, O., Aumont, O., Balkanski, Y., Bekki, S., Bellenger, H., Benshila, R., Bony, S., Bopp, L., Braconnot, P., Brockmann, P., Cadule, P., Cheruy, F., Codron, F., Cozic, A., Cugnet, D., de Noblet, N., Duvel, J.-P., Ethé, P., Fairhead, L., Fichefet, T., Flavoni, S., Friedlingstein, P., Grandpeix, J.-Y., Guez, L., Guilyardi, E., Hauglustaine, D., Hourdin, F., Idelkadi, A., Ghattas, J., Joussaume, S., Kageyama, M., Krinner, G., Labetoulle, S., Lahellec, A., Lefebvre, M.-P., Lefevre, F., Levy, C., Li, Z. X., Lloyd, J., Lott, F., Madec, G., Mancip, M., Marchand, M., Masson, S., Meurdesoif, Y., Mignot, J., Musat, I., Parouty, S., Polcher, J., Rio, C., Schulz, M., Swingedouw, D., Szopa, S., Talandier, C., Terray, P., Viovy, N., and Vuichard, N.: Climate change projections using the IPSL-CM5 Earth System Model: from CMIP3 to CMIP5, Clim. Dynamics, 40, 2123–2165, https://doi.org/10.1007/s00382-012-1636-1, 2013.

Dunne, J. P., John, J. G., Adcroft, A. J., Griffies, S. M., Hallberg, R. W., Shevliakova, E. N., Stouffer, R. J., Cooke, W., Dunne, K. A., Harrison, M. J., Krasting, J. P., Malyshev, S. L., Milly, P. C. D., Phillips, P. J., Sentman, L. T., Samuels, B. L., Spelman, M., Winton, M., Wittenberg, A. T., and Zadeh, N.: GFDL's ESM2 global coupled climate-carbon Earth System Models Part I: Physical Formulation and Baseline Simulation Characteristics, J. Climate, 25, https://doi.org/10.1175/JCLI-D-11-00560.1, 2013a.

Dunne, J. P., John, J. G., Adcroft, A. J., Griffies, S. M., Hallberg, R. W., Shevliakova, E. N., Stouffer, R. J., Cooke, W., Dunne, K. A., Harrison, M. J., Krasting, J. P., Malyshev, S. L., Milly, P. C. D., Phillips, P. J., Sentman, L. T., Samuels, B. L., Spelman, M., Winton, M., Wittenberg, A. T., and Zadeh, N.: GFDL's ESM2 global coupled climate-carbon Earth System Models Part II: Carbon System Formulation and Baseline Simulation Characteristics, J. Climate, 26, https://doi.org/10.1175/JCLI-D-12-00150.1, 2013b.

Fassbender, A. J., Orr, J. C., and Dickson, A. G.: Technical note: Interpreting pH changes, Biogeosciences, 18, 1407–1415, https://doi.org/10.5194/bg-18-1407-2021, https://bg.copernicus.org/articles/18/1407/2021/, 2021.

Friedlingstein, P., O'Sullivan, M., Jones, M. W., Andrew, R. M., Hauck, J., Olsen, A., Peters, G. P., Peters, W., Pongratz, J., Sitch, S., Le Quéré, C., Canadell, J. G., Ciais, P., Jackson, R. B., Alin, S., Aragão, L. E. O. C., Arneth, A., Arora, V., Bates, N. R., Becker, M., Benoit-Cattin, A., Bittig, H. C., Bopp, L., Bultan, S., Chandra, N., Chevallier, F., Chini, L. P., Evans, W., Florentie, L., Forster, P. M., Gasser, T., Gehlen, M., Gilfillan, D., Gkritzalis, T., Gregor, L., Gruber, N., Harris, I., Hartung, K., Haverd, V., Houghton, R. A., Ilyina, T., Jain, A. K., Joetzjer, E., Kadono, K., Kato, E., Kitidis, V., Korsbakken, J. I., Landschützer, P., Lefèvre, N., Lenton, A., Lienert, S., Liu, Z., Lombardozzi, D., Marland, G., Metzl, N., Munro, D. R., Nabel, J. E. M. S., Nakaoka, S.-I., Niwa, Y., O'Brien, K., Ono, T., Palmer, P. I., Pierrot, D., Poulter, B., Resplandy, L., Robertson, E., Rödenbeck, C., Schwinger, J., Séférian, R., Skjelvan, I., Smith, A. J. P., Sutton, A. J., Tanhua, T., Tans, P. P., Tian, H., Tilbrook, B., van der Werf, G., Vuichard, N., Walker, A. P., Wanninkhof, R., Watson, A. J., Willis, D., Wiltshire, A. J., Yuan, W., Yue, X., and Zaehle, S.: Global Carbon Budget 2020, Earth System Science Data, 12, 3269–3340, https://doi.org/10.5194/essd-12-3269-2020, https://essd.copernicus.org/articles/12/3269/2020/, 2020.

Frölicher, T. L., Rodgers, K. B., Stock, C. A., and Cheung, W. W. L.: Sources of uncertainties in 21st century projections of potential ocean ecosystem stressors, Global Biogeochemical Cycles, 30, 1224–1243, https://doi.org/https://doi.org/10.1002/2015GB005338, https://agupubs.onlinelibrary.wiley.com/doi/abs/10.1002/2015GB005338, 2016.

García-Ibáñez, M. I., Bates, N. R., Bakker, D. C., Fontela, M., and Velo, A.: Cold-water corals in the Subpolar North Atlantic Ocean exposed to aragonite undersaturation if the 2 °C global warming target is not met, Global and Planetary Change, 201, 103 480, https://doi.org/https://doi.org/10.1016/j.gloplacha.2021.103480, https://www.sciencedirect.com/science/article/pii/S0921818121000655, 2021.

Gattuso, J.-P. and Hansson, L.: Ocean acidification: background and history, In Ocean Acidification, ed. J-P Gattuso, L Hansson, pp. 1–20, Oxford University Press, Oxford, UK, 2011.

Giorgetta, M. A., Jungclaus, J., Reick, C. H., Legutke, S., Bader, J., Böttinger, M., Brovkin, V., Crueger, T., Esch, M., Fieg, K., Glushak, K., Gayler, V., Haak, H., Hollweg, H.-D., Ilyina, T., Kinne, S., Kornblueh, L., Matei, D., Mauritsen, T., Mikolajewicz, U., Mueller, W., Notz, D., Pithan, F., Raddatz, T., Rast, S., Redler, R., Roeckner, E., Schmidt, H., Schnur, R., Segschneider, J., Six, K. D., Stockhause, M., Timmreck, C., Wegner, J., Widmann, H., Wieners, K.-H., Claussen, M., Marotzke, J., and Stevens, B.: Climate and carbon cycle changes from 1850 to 2100 in MPI-ESM simulations for the Coupled Model Intercomparison Project phase 5, Journal of Advances in Modeling Earth Systems, 5, 572–597, https://doi.org/10.1002/jame.20038, 2013.

Giraudeau, J., Hulot, V., Hanquiez, V., Devaux, L., Howa, H., and Garlan, T.: A survey of the summer coccolithophore community in the western Barents Sea, Journal of Marine Systems, 158, 93–105, https://doi.org/https://doi.org/10.1016/j.jmarsys.2016.02.012, https://www.sciencedirect.com/science/article/pii/S0924796316300021, 2016.

Guinotte, J. M., Orr, J., Cairns, S., Freiwald, A., Morgan, L., and George, R.: Will human-induced changes in seawater chemistry alter the distribution of deep-sea scleractinian corals?, Frontiers in Ecology and the Environment, 4, 141–146, https://doi.org/10.1890/1540-9295(2006)004[0141:WHCISC]2.0.CO;2, 2006.

He, Y.-C., Tjiputra, J., Langehaug, H. R., Jeansson, E., Gao, Y., Schwinger, J., and Olsen, A.: A Model-Based Evaluation of the Inverse Gaussian Transit-Time Distribution Method for Inferring Anthropogenic Carbon Storage in the Ocean, Journal of Geophysical Research: Oceans, 123, 1777–1800, https://doi.org/https://doi.org/10.1002/2017JC013504, https://agupubs.onlinelibrary.wiley.com/doi/abs/10.1002/2017JC013504, 2018.

Hennige, S. J., Wicks, L. C., Kamenos, N. A., Perna, G., Findlay, H. S., and Roberts, J. M.: Hidden impacts of ocean acidification to live and dead coral framework, Proceedings of the Royal Society B: Biological Sciences, 282, 20150 990, https://doi.org/10.1098/rspb.2015.0990, https://royalsocietypublishing.org/doi/abs/10.1098/rspb.2015.0990, 2015.

Holliday, N. P., Hughes, S. L., Bacon, S., Beszczynska-Möller, A., Hansen, B., Lavín, A., Loeng, H., Mork, K. A., Østerhus, S., Sherwin, T., and Walczowski, W.: Reversal of the 1960s to 1990s freshening trend in the northeast North Atlantic and Nordic Seas, Geophysical Research Letters, 35, https://doi.org/10.1029/2007GL032675, https://agupubs.onlinelibrary.wiley.com/doi/abs/10.1029/2007GL032675, 2008.

Jeansson, E., Olsen, A., and Jutterström, S.: Arctic Intermediate Water in the Nordic Seas, 1991–2009, Deep Sea Research Part I: Oceanographic Research Papers, 128, 82 – 97, https://doi.org/https://doi.org/10.1016/j.dsr.2017.08.013, http://www.sciencedirect.com/science/article/pii/S0967063716300668, 2017.

Jeansson, E., Olsen, A., Lauvset, S. K., Brakstad, A., Jackson, K., Lunde, L. F., He, Y., and Onarheim, T.: Discrete profile measurements of dissolved inorganic carbon, total alkalinity, other hydrographic and chemical data obtained during the R/V G.O. Sars Repeat Hydrography Cruise in the Greenland Sea and Iceland Sea: GO-SHIP Section 75N (EXPOCODE 58GS20160802), from 2016-08-02 to 2016-08-12 (NCEI Accession 0174834). NOAA National Centers for Environmental Information., https://doi.org/10.25921/3kjg-ak47., dataset, 2018.

Jiang, L.-Q., Carter, B. R., Feely, R. A., Lauvset, S. K., and Olsen, A.: Surface ocean pH and buffer capacity: past, present and future, Scientific Reports, 9, 18 624, https://doi.org/10.1038/s41598-019-55039-4, https://doi.org/10.1038/s41598-019-55039-4, 2019.

Johannessen, T.: Dissolved inorganic carbon, alkalinity, temperature, salinity and other variables collected from discrete sample and profile observations using CTD, bottle and other instruments from the HAKON MOSBY in the North Greenland Sea from 1996-11-21 to 1996-11-30 (NCEI Accession 0113544). NOAA National Centers for Environmental Information., https://doi.org/10.3334/cdiac/otg.carina$_5$8aa19961121, $dataset$, 2013a.

Johannessen, T.: Dissolved inorganic carbon, alkalinity, temperature, salinity and other variables collected from discrete sample and profile observations using CTD, bottle and other instruments from the HAKON MOSBY in the North Greenland Sea and Norwegian Sea from 1997-02-25 to 1997-03-24 (NCEI Accession 0113545). NOAA National Centers for Environmental Information., https://doi.org/10.3334/cdiac/otg.carina$_5$8aa19970225, $dataset$, 2013b.

Johannessen, T. and Golmen, L. G.: Dissolved inorganic carbon, alkalinity, temperature, salinity and other variables collected from discrete sample and profile observations using CTD, bottle and other instruments from the HAKON MOSBY in the North Greenland Sea and Norwegian Sea from 1994-08-26 to 1994-09-10 (NCEI Accession 0113542). NOAA National Centers for Environmental Information., https://doi.org/10.3334/cdiac/otg.carina$_5$8aa19940826, $dataset$, 2013.

Johannessen, T. and Olsen, A.: Dissolved inorganic carbon, alkalinity, temperature, salinity and other variables collected from discrete sample and profile observations during the G.O. SARS cruise along GO-SHIP Repeat Section A75N (EXPOCODE 58GS200309) in the North Atlantic Ocean, North Greenland Sea and Norwegian Sea from 2003-09-22 to 2003-10-13 (NCEI Accession 0113752). NOAA National Centers for Environmental Information., https://doi.org/10.3334/cdiac/otg.carina$_5$8gs20030922, $dataset$, 2013.

Johannessen, T. and Simonsen, K. .: Dissolved inorganic carbon, alkalinity, temperature, salinity and other variables collected from discrete sample and profile observations using CTD, bottle and other instruments from the HAKON MOSBY in the North Greenland Sea and Norwegian Sea from 1998-03-08 to 1998-03-24 (NCEI Accession 0113546). NOAA National Centers for Environmental Information., https://doi.org/10.3334/cdiac/otg.carina$_5$8aa19980308, $dataset$, 2013.

Johannessen, T., Skjelvan, I., and Rey, F.: Dissolved inorganic carbon, alkalinity, temperature, salinity and other variables collected from discrete sample and profile observations using CTD, bottle and other instruments from the JOHAN HJORT in the North Greenland Sea and Norwegian Sea from 1994-05-25 to 1994-06-06 (NCEI Accession 0113954). NOAA National Centers for Environmental Information., https://doi.org/10.3334/cdiac/otg.carina$_5$8jh19940525, $dataset$, 2013a.

Johannessen, T., Skjelvan, I., and Watson, A. J.: Dissolved inorganic carbon, alkalinity, temperature, salinity and other variables collected from discrete sample and profile observations using CTD, bottle and other instruments from the JAMES CLARK ROSS in the North Greenland Sea and Norwegian Sea from 1996-07-20 to 1996-08-22 (NCEI Accession 0113757). NOAA National Centers for Environmental Information. Dataset., https://doi.org/10.3334/cdiac/otg.carina$_7$4jc19960720., $dataset$, 2013b.

Johannessen, T., Soiland, H., Thingstad, T. F., Bellerby, R. G. J., and Olsen, A.: Dissolved inorganic carbon, alkalinity, temperature, salinity and other variables collected from discrete sample and profile observations using CTD, bottle and other instruments from the G.O. SARS in the Barents Sea, North Atlantic Ocean and others from 2009-05-28 to 2009-08-11 (NCEI Accession 0114433). NOAA National Centers for Environmental Information., https://doi.org/10.25921/3q88-gs40, dataset, 2013c.

Jones, E., Chierici, M., Skjelvan, I., M. Norli, K. B., Lødemel, H., Kutti, T., Sørensen, K., King, A., Jackson, K., and de Lange, T.: Monitoring of the ocean acidification in Norwegian seas in 2017, Report, Miljødirektoratet, M-1072, Tech. rep., 2018.

Jones, E., Chierici, M., Skjelvan, I., Norli, M., Børsheim, K., Lødemel, H., Sørensen, K., King, A., Lauvset, S., Jackson, K., de Lange, T., Johannsessen, T., and Mourgues, C.: Monitoring ocean acidification in Norwegian seas in 2018, Rapport, Miljødirektoratet, M-1417, Tech. rep., 2019.

Jones, E., Chierici, M., Skjelvan, I., Norli, M., Frigstad, H., Børsheim, K., Lødemel, H., Kutti, T., King, A., Sørensen, K., Lauvset, S., Jackson-Misje, K., Apelthun, L., de Lange, T., Johannsessen, T., Mourgues, C., and Bellerby, R.: Monitoring ocean acidification in Norwegian seas in 2019, Rapport, Miljødirektoratet, M-1735, Tech. rep., 2020.

Jones, E. P., Azetsu-Scott, K., Aagaard, K., Carmack, E., and Swift, J. H.: Dissolved inorganic carbon, alkalinity, temperature, salinity and other variables collected from discrete sample and profile observations using CTD, bottle and other instruments from the LOUIS S. ST. LAURENT in the Arctic Ocean, Beaufort Sea and North Greenland Sea from 1994-07-24 to 1994-09-01 (NCEI Accession 0113983).NOAA National Centers for Environmental Information., https://doi.org/10.3334/cdiac/otg.carina$_1$8sn19940724, $dataset$, 2013.

Jutterström, S. and Jeansson, E.: Anthropogenic carbon in the East Greenland Current, Progress in Oceanography, 78, 29 – 36, https://doi.org/https://doi.org/10.1016/j.pocean.2008.04.001, http://www.sciencedirect.com/science/article/pii/S0079661108000876, 2008.

Karstensen, J., Schlosser, P., Wallace, D. W. R., Bullister, J. L., and Blindheim, J.: Water mass transformation in the Greenland Sea during the 1990s, Journal of Geophysical Research: Oceans, 110, https://doi.org/https://doi.org/10.1029/2004JC002510, https://agupubs.onlinelibrary.wiley.com/doi/abs/10.1029/2004JC002510, 2005.

Kutti, T., Bergstad, O. A., Fosså, J. H., and Helle, K.: Cold-water coral mounds and sponge-beds as habitats for demersal fish on the Norwegian shelf, Deep Sea Research Part II: Topical Studies in Oceanography, 99, 122 – 133, https://doi.org/https://doi.org/10.1016/j.dsr2.2013.07.021, http://www.sciencedirect.com/science/article/pii/S0967064513002956, biology and Geology of Deep-Sea Coral Ecosystems: Proceedings of the Fifth International Symposium on Deep Sea Corals, 2014.

Kwiatkowski, L. and Orr, J. C.: Diverging seasonal extremes for ocean acidification during the twenty-first century, Nature Climate Change, 8, 141–145, https://doi.org/10.1038/s41558-017-0054-0, https://doi.org/10.1038/s41558-017-0054-0, 2018.

Kwiatkowski, L., Torres, O., Bopp, L., Aumont, O., Chamberlain, M., Christian, J. R., Dunne, J. P., Gehlen, M., Ilyina, T., John, J. G., Lenton, A., Li, H., Lovenduski, N. S., Orr, J. C., Palmieri, J., Santana-Falcón, Y., Schwinger, J., Séférian, R., Stock, C. A., Tagliabue, A., Takano, Y., Tjiputra, J., Toyama, K., Tsujino, H., Watanabe, M., Yamamoto, A., Yool, A., and Ziehn, T.: Twenty-first century ocean warming, acidification, deoxygenation, and upper-ocean nutrient and primary production decline from CMIP6 model projections, Biogeosciences, 17, 3439–3470, https://doi.org/10.5194/bg-17-3439-2020, https://bg.copernicus.org/articles/17/3439/2020/, 2020.

Lauvset, S. K., Gruber, N., Landschützer, P., Olsen, A., and Tjiputra, J.: Trends and drivers in global surface ocean pH over the past 3 decades, Biogeosciences, 12, 1285–1298, https://doi.org/10.5194/bg-12-1285-2015, https://bg.copernicus.org/articles/12/1285/2015/, 2015.

Lauvset, S. K., Key, R. M., Olsen, A., van Heuven, S., Velo, A., Lin, X., Schirnick, C., Kozyr, A., Tanhua, T., Hoppema, M., Jutterström, S., Steinfeldt, R., Jeansson, E., Ishii, M., Perez, F. F., Suzuki, T., and Watelet, S.: A new global interior ocean mapped climatology: the $1^\circ \times 1^\circ$ GLODAP version 2, Earth System Science Data, 8, 325–340, https://doi.org/10.5194/essd-8-325-2016, https://essd.copernicus.org/articles/8/325/2016/, 2016.

Lauvset, S. K., Brakstad, A., Våge, K., Olsen, A., Jeansson, E., and Mork, K. A.: Continued warming, salinification and oxygenation of the Greenland Sea gyre, Tellus A: Dynamic Meteorology and Oceanography, 70, 1–9, https://doi.org/10.1080/16000870.2018.1476434, https://doi.org/10.1080/16000870.2018.1476434, 2018.

Lauvset, S. K., Carter, B. R., Pèrez, F. F., Jiang, L.-Q., Feely, R. A., Velo, A., and Olsen, A.: Processes Driving Global Interior Ocean pH Distribution, Global Biogeochemical Cycles, 34, e2019GB006 229, https://doi.org/https://doi.org/10.1029/2019GB006229, https://agupubs.onlinelibrary.wiley.com/doi/abs/10.1029/2019GB006229, e2019GB006229 2019GB006229, 2020.

Lefèvre, N., Watson, A. J., Olsen, A., Ríos, A. F., Pérez, F. F., and Johannessen, T.: A decrease in the sink for atmospheric CO_2 in the North Atlantic, Geophysical Research Letters, 31, https://doi.org/10.1029/2003GL018957, https://agupubs.onlinelibrary.wiley.com/doi/abs/10.1029/2003GL018957, 2004.

Lenton, A., Metzl, N., Takahashi, T., Kuchinke, M., Matear, R. J., Roy, T., Sutherland, S. C., Sweeney, C., and Tilbrook, B.: The observed evolution of oceanic pCO2 and its drivers over the last two decades, Global Biogeochemical Cycles, 26, https://doi.org/https://doi.org/10.1029/2011GB004095, https://agupubs.onlinelibrary.wiley.com/doi/abs/10.1029/2011GB004095, 2012.

Lewis, E. and Wallace, D. W. R.: Program Developed for CO_2 System Calculations, ORNL/CDIAC-105. Carbon Dioxide Information Analysis Center, Oak Ridge National Laboratory, US Department of Energy, Oak Ridge, Tennessee., 1998.

Long, M. C., Lindsay, K., Peacock, S., Moore, J. K., and Doney, S. C.: Twentieth-century oceanic carbon uptake and storage in CESM1(BGC), J. Climate, 26, 6775–6800, https://doi.org/http://dx.doi.org/10.1175/JCLI-D-12-00184.1, 2013.

Lueker, T. J., Dickson, A. G., and Keeling, C. D.: Ocean pCO_2 calculated from dissolved inorganic carbon, alkalinity, and equations for K1 and K2: validation based on laboratory measurements of CO_2 in gas and seawater at equilibrium, Marine Chemistry, 70, 105 – 119, https://doi.org/https://doi.org/10.1016/S0304-4203(00)00022-0, http://www.sciencedirect.com/science/article/pii/S0304420300000220, 2000.

Maier-Reimer, E., Kriest, I., Segschneider, J., and Wetzel, P.: The HAMburg Ocean Carbon Cycle Model HAMOCC5.1 - Technical Description Release 1.1.Berichte zur Erdsystemforschung, 14., Tech. rep., 2005.

Manno, C., Bednaršek, N., Tarling, G. A., Peck, V. L., Comeau, S., Adhikari, D., Bakker, D. C., Bauerfeind, E., Bergan, A. J., Berning, M. I., Buitenhuis, E., Burridge, A. K., Chierici, M., Flöter, S., Fransson, A., Gardner, J., Howes, E. L., Keul, N., Kimoto, K., Kohnert, P., Lawson, G. L., Lischka, S., Maas, A., Mekkes, L., Oakes, R. L., Pebody, C., Peijnenburg, K. T., Seifert, M., Skinner, J., Thibodeau, P. S.,

Wall-Palmer, D., and Ziveri, P.: Shelled pteropods in peril: Assessing vulnerability in a high CO2 ocean, Earth-Science Reviews, 169, 132–145, https://doi.org/https://doi.org/10.1016/j.earscirev.2017.04.005, https://www.sciencedirect.com/science/article/pii/S0012825216302495, 2017.

Marcussen, Christian; Anderson, L. G.: Discrete profile measurements of carbon dioxide, hydrographic and chemical data during the R/V Oden Lomonosov Ridge off Greenland (LOMROG) expedition (EXPOCODE 77DN20070812) in the Arctic Ocean from 2007-08-12 to 2007-09-19 (NCEI Accession 0170966). NOAA National Centers for Environmental Information., https://doi.org/10.7289/v52n50jb., dataset, 2018.

McCulloch, M., Trotter, J., Montagna, P., Falter, J., Dunbar, R., Freiwald, A., Försterra, G., López Correa, M., Maier, C., Rüggeberg, A., and Taviani, M.: Resilience of cold-water scleractinian corals to ocean acidification: Boron isotopic systematics of pH and saturation state up-regulation, Geochimica et Cosmochimica Acta, 87, 21 – 34, https://doi.org/https://doi.org/10.1016/j.gca.2012.03.027, http://www.sciencedirect.com/science/article/pii/S001670371200169X, 2012.

Meinshausen, M., Smith, S. J., Calvin, K., Daniel, J. S., Kainuma, M. L. T., Lamarque, J.-F., Matsumoto, K., Montzka, S. A., Raper, S. C. B., Riahi, K., Thomson, A., Velders, G. J. M., and van Vuuren, D. P. P.: The RCP greenhouse gas concentrations and their extensions from 1765 to 2300, Climatic Change, 109, 213, https://doi.org/10.1007/s10584-011-0156-z, https://doi.org/10.1007/s10584-011-0156-z, 2011.

Messias, M.-J., Watson, A., Johannessen, T., Oliver, K., Olsson, K., Fogelqvist, E., Olafsson, J., Bacon, S., Balle, J., Bergman, N., Budéus, G., Danielsen, M., Gascard, J.-C., Jeansson, E., Olafsdottir, S., Simonsen, K., Tanhua, T., Van Scoy, K., and Ledwell, J.: The Greenland Sea tracer experiment 1996–2002: Horizontal mixing and transport of Greenland Sea Intermediate Water, Progress in Oceanography, 78, 85 – 105, https://doi.org/https://doi.org/10.1016/j.pocean.2007.06.005, http://www.sciencedirect.com/science/article/pii/S0079661108000852, 2008.

Metzl, N., Corbière, A., Reverdin, G., Lenton, A., Takahashi, T., Olsen, A., Johannessen, T., Pierrot, D., Wanninkhof, R., Ólafsdóttir, S. R., Olafsson, J., and Ramonet, M.: Recent acceleration of the sea surface fCO_2 growth rate in the North Atlantic subpolar gyre (1993–2008) revealed by winter observations, Global Biogeochemical Cycles, 24, https://doi.org/10.1029/2009GB003658, https://agupubs.onlinelibrary.wiley.com/doi/abs/10.1029/2009GB003658, 2010.

NOAA National Geophysical Data Center: ETOPO1 1 Arc-Minute Global Relief Model. NOAA National Centers for Environmental Information., doi:10.7289/V5C8276M, dataset, 2020.

Ólafsdóttir, S. R., Benoit-Cattin, A., and Danielsen, M.: Dissolved inorganic carbon (DIC), total alkalinity, temperature, salinity, nutrients and dissolved oxygen collected from discrete samples and profile observations during the R/Vs Arni Fridriksson and Bjarni Saemundsson time series IcelandSea (LN6) cruises in the North Atlantic Ocean from 2014-02-18 to 2019-10-31 (NCEI Accession 0209074), https://doi.org/10.25921/qhed-3h84, dataset, 2020.

Ólafsson, J.: Winter mixed layer nutrients in the Irminger and Iceland Seas,1990-2000, ICES Marine Science Symposia, 219, 2003.

Ólafsson, J.: Partial pressure (or fugacity) of carbon dioxide, dissolved inorganic carbon, temperature, salinity and other variables collected from discrete samples, profile and time series profile observations during the R/Vs Arni Fridriksson and Bjarni Saemundsson time series IcelandSea (LN6) cruises in the North Atlantic Ocean from 1985-02-22 to 2013-11-26 (NCEI Accession 0100063), https://doi.org/10.3334/cdiac/otg.carina_icelandsea, dataset, 2012.

Ólafsson, J., Ólafsdóttir, S., Benoit-Cattin, A., Danielsen, M., Arnarson, T. S., and Takahashi, T.: Rate of Iceland Sea acidification from time series measurements, Biogeosciences, 6, 2661–2668, 2009.

Ólafsson, J., Lee, K., Ólafsdóttir, S. R., Benoit-Cattin, A., Lee, C.-H., and Kim, M.: Boron to salinity ratios for Atlantic, Arctic and Polar Waters: A view from downstream, Marine Chemistry, 224, 103 809, https://doi.org/https://doi.org/10.1016/j.marchem.2020.103809, http://www.sciencedirect.com/science/article/pii/S0304420320300633, 2020a.

Ólafsson, J., Ólafsdóttir, S. R., Takahashi, T., Danielsen, M., and Arnarson, T. S.: Enhancement of the North Atlantic CO_2 sink by Arctic Waters, Biogeosciences Discussions, 2020, 1–21, https://doi.org/10.5194/bg-2020-313, https://bg.copernicus.org/preprints/bg-2020-313/, 2020b.

Olsen, A. and Omar, A. M.: Dissolved inorganic carbon, alkalinity, temperature, salinity and other variables collected from discrete sample and profile observations using Alkalinity titrator, CTD and other instruments from the G.O. SARS in the North Greenland Sea and Norwegian Sea from 2006-07-21 to 2006-08-05 (NCEI Accession 0105859). NOAA National Centers for Environmental Information., https://doi.org/10.3334/cdiac/otg.clivar$_7$5$n_2$006, $dataset$, 2013.

Olsen, A., Johannessen, T., and Rey, F.: On the nature of the factors that control spring bloom development at the entrance to the Barents Sea and their interannual variability, Sarsia, 88, 379–393, https://doi.org/10.1080/00364820310003145, https://doi.org/10.1080/00364820310003145, 2003.

Olsen, A., Omar, A. M., Bellerby, R. G. J., Johannessen, T., Ninnemann, U., Brown, K. R., Olsson, K. A., Olafsson, J., Nondal, G., Kivimäe, C., Kringstad, S., Neill, C., and Olafsdottir, S.: Magnitude and origin of the anthropogenic CO_2 increase and 13C Suess effect in the Nordic seas since 1981, Global Biogeochemical Cycles, 20, https://doi.org/10.1029/2005GB002669, https://agupubs.onlinelibrary.wiley.com/doi/abs/10.1029/2005GB002669, 2006.

Olsen, A., Brown, K. R., Chierici, M., Johannessen, T., and Neill, C.: Sea-surface CO_2 fugacity in the subpolar North Atlantic, Biogeosciences, 5, 535–547, https://doi.org/10.5194/bg-5-535-2008, https://bg.copernicus.org/articles/5/535/2008/, 2008.

Olsen, A., Omar, A. M., and Johannessen, T.: Dissolved inorganic carbon, alkalinity, temperature, salinity and other variables collected from discrete sample and profile observations using CTD, bottle and other instruments from the HAKON MOSBY in the North Atlantic Ocean, North Greenland Sea and Norwegian Sea from 2001-05-27 to 2001-06-19 (NCEI Accession 0113754). NOAA National Centers for Environmental Information., https://doi.org/10.3334/cdiac/otg.carina$_5$8aa20010527, $dataset$, 2013.

Olsen, A., Lange, N., Key, R. M., Tanhua, T., Álvarez, M., Becker, S., Bittig, H. C., Carter, B. R., Cotrim da Cunha, L., Feely, R. A., van Heuven, S., Hoppema, M., Ishii, M., Jeansson, E., Jones, S. D., Jutterström, S., Karlsen, M. K., Kozyr, A., Lauvset, S. K., Lo Monaco, C., Murata, A., Pérez, F. F., Pfeil, B., Schirnick, C., Steinfeldt, R., Suzuki, T., Telszewski, M., Tilbrook, B., Velo, A., and Wanninkhof, R.: GLODAPv2.2019 – an update of GLODAPv2, Earth System Science Data, 11, 1437–1461, https://doi.org/10.5194/essd-11-1437-2019, https://essd.copernicus.org/articles/11/1437/2019/, 2019.

Omar, A. M. and Olsen, A.: Dissolved inorganic carbon, alkalinity, temperature, salinity and other variables collected from discrete sample and profile observations using CTD, bottle and other instruments from the HAKON MOSBY in the Barents Sea, North Greenland Sea and Norwegian Sea from 1999-10-03 to 1999-10-11 (NCEI Accession 0113888). NOAA National Centers for Environmental Information., https://doi.org/10.3334/cdiac/otg.carina$_5$8aa19991003., $dataset$, 2013.

Omar, A. M. and Skogseth, R.: Dissolved inorganic carbon, alkalinity, temperature, salinity and other variables collected from discrete sample and profile observations using CTD, bottle and other instruments from the HAKON MOSBY in the Barents Sea and Norwegian Sea from 2001-08-22 to 2001-08-29 (NCEI Accession 0113887). NOAA National Centers for Environmental Information., https://doi.org/10.3334/cdiac/otg.carina$_5$8aa20010822, $dataset$, 2013.

Omar, Abdirahman M.; Østerhus, S.: Dissolved inorganic carbon, alkalinity, temperature, salinity and other variables collected from discrete sample and profile observations using CTD, bottle and other instruments from the HAKON MOSBY in the Barents Sea from 2000-09-23 to 2000-10-03 (NCEI Accession 0113886). NOAA National Centers for Environmental Information, https://doi.org/10.3334/cdiac/otg.carina$_5$8aa20000923, $dataset$, 2013.

Orr, J. C.: Recent and future changes in ocean carbonate chemistry, In Ocean Acidification, ed. J-P Gattuso, L Hansson, pp. 41–66, Oxford University Press, Oxford, UK, 2011.

Orr, J. C., Fabry, V. J., Aumont, O., Bopp, L., Doney, S. C., Feely, R. A., Gnanadesikan, A., Gruber, N., Ishida, A., Joos, F., Key, R. M., Lindsay, K., Maier-Reimer, E., Matear, R., Monfray, P., Mouchet, A., Najjar, R. G., Plattner, G.-K., Rodgers, K. B., Sabine, C. L., Sarmiento, J. L., Schlitzer, R., Slater, R. D., Totterdell, I. J., Weirig, M.-F., Yamanaka, Y., and Yool, A.: Anthropogenic ocean acidification over the twenty-first century and its impact on calcifying organisms, Nature, 437, 681–686, https://doi.org/10.1038/nature04095, https://doi.org/10.1038/nature04095, 2005.

Orr, J. C., Epitalon, J.-M., Dickson, A. G., and Gattuso, J.-P.: Routine uncertainty propagation for the marine carbon dioxide system, Marine Chemistry, 207, 84–107, https://doi.org/https://doi.org/10.1016/j.marchem.2018.10.006, https://www.sciencedirect.com/science/article/pii/S030442031830149X, 2018.

Østerhus, S. and Gammelsrød, T.: The Abyss of the Nordic Seas Is Warming, Journal of Climate, 12, 3297–3304, https://doi.org/10.1175/1520-0442(1999)012<3297:TAOTNS>2.0.CO;2, https://doi.org/10.1175/1520-0442(1999)012<3297:TAOTNS>2.0.CO;2, 1999.

Oziel, L., Baudena, A., Ardyna, M., Massicotte, P., Randelhoff, A., Sallée, J.-B., Ingvaldsen, R. B., Devred, E., and Babin, M.: Faster Atlantic currents drive poleward expansion of temperate phytoplankton in the Arctic Ocean, Nature Communications, 11, 1705, https://doi.org/10.1038/s41467-020-15485-5, https://doi.org/10.1038/s41467-020-15485-5, 2020.

Pegler, K., Graf, G., and Pfannkuche, O.: Partial pressure (or fugacity) of carbon dioxide, dissolved inorganic carbon, alkalinity, temperature, salinity and other variables collected from discrete sample and profile observations using CTD, bottle and other instruments from the METEOR in the North Atlantic Ocean, North Greenland Sea and Norwegian Sea from 1992-07-01 to 1992-08-31 (NCEI Accession 0113985). NOAA National Centers for Environmental Information., https://doi.org/10.3334/cdiac/otg.carina$_0$6mt19920701, $dataset$, 2013.

Perez, F. F., Fontela, M., García-Ibáñez, M. I., Mercier, H., Velo, A., Lherminier, P., Zunino, P., de la Paz, M., Alonso-Pérez, F., Guallart, E. F., and Padin, X. A.: Meridional overturning circulation conveys fast acidification to the deep Atlantic Ocean, Nature, 554, 515–518, https://doi.org/10.1038/nature25493, https://doi.org/10.1038/nature25493, 2018.

Raven, J., Caldeira, K., Elderfield, H., Hoegh-Guldberg, O., Liss, P., Riebesell, U., Shepherd, J., Turley, C., and Watson, A.: Ocean acidification due to increasing atmospheric carbon dioxide, Policy document, The Royal Society, London Pp. 1–68, 2005.

Ruiz-Barradas, A., Chafik, L., Nigam, S., and Häkkinen, S.: Recent subsurface North Atlantic cooling trend in context of Atlantic decadal-to-multidecadal variability, Tellus A: Dynamic Meteorology and Oceanography, 70, 1–19, https://doi.org/10.1080/16000870.2018.1481688, https://doi.org/10.1080/16000870.2018.1481688, 2018.

Sarmiento, J. L. and Gruber, N.: Ocean Biogeochemical Dynamics, chap. 8, pp. 318–358, Princeton University Press, Princeton, Woodstock, 2006.

Schauer, U., Jones, E. M., Ulfsbo, A., Hansell, D. A., Smethie, William M., J., Rabe, B., and van Ooijen, J. C.: Discrete, profile measurements of the dissolved inorganic carbon (DIC), total alkalinity, pH on total scale and other hydrographic and chemical data obtained during the PS-94, ARK-XXIX/3, TransArc-II cruise onboard the R/V Polarstern (EXPOCODE 06AQ20150817) in the central Arctic Ocean from 2015-08-17 to 2015-10-15 (NCEI Accession 0170256). NOAA National Centers for Environmental Information., https://doi.org/10.7289/v5319t5z, dataset, 2018.

Shu, Q., Qiao, F., Song, Z., Zhao, J., and Li, X.: Projected Freshening of the Arctic Ocean in the 21st Century, Journal of Geophysical Research: Oceans, 123, 9232–9244, https://doi.org/10.1029/2018JC014036, https://agupubs.onlinelibrary.wiley.com/doi/abs/10.1029/2018JC014036, 2018.

Skjelvan, I., Falck, E., Rey, F., and Kringstad, S. B.: Inorganic carbon time series at Ocean Weather Station M in the Norwegian Sea, Biogeosciences, 5, 549–560, https://doi.org/10.5194/bg-5-549-2008, https://bg.copernicus.org/articles/5/549/2008/, 2008.

Skjelvan, I., Johannessen, T., and Anderson, L. G.: Dissolved inorganic carbon, alkalinity, temperature, salinity and other variables collected from discrete sample and profile observations using CTD, bottle and other instruments from the HAKON MOSBY in the North Greenland Sea and Norwegian Sea from 1994-02-24 to 1994-03-17 (NCEI Accession 0113541). NOAA National Centers for Environmental Information. Dataset., https://doi.org/10.3334/cdiac/otg.carina$_5$8aa19940224, $dataset$, 2013.

Skjelvan, I., Jeansson, E., Chierici, M., Omar, A., Olsen, A., Lauvset, S., and Johannessen, T.: Havforsuring og opptak av antropogent karbon i de Nordiske hav [Ocean acidification and uptake of anthropogenic carbon in the Nordic Seas], 1981-2013. Miljødirektoratet, Rapport M244-2014, Tech. rep., 2014.

Skjelvan, I., Jones, E., Chierici, M., Frigstad, H., Børsheim, K., Lødemel, H., Kutti, T., King, A., Sørensen, K., Omar, A., Bellerby, R., Christensen, G., Marty, S., Protsenko, E., Mengeot, C., Valestrand, L., Norli, M., Jackson-Misje, K., Apelthun, L., de Lange, T., Johannessen, T., and Mourgues., C.: Monitoring of the ocean acidification in Norwegian seas in 20202, Report, Miljødirektoratet, M-2056, Tech. rep., 2021.

Skogen, M. D., Olsen, A., Børsheim, K. Y., Sandø, A. B., and Skjelvan, I.: Modelling ocean acidification in the Nordic and Barents Seas in present and future climate, Journal of Marine Systems, 131, 10–20, https://doi.org/https://doi.org/10.1016/j.jmarsys.2013.10.005, https://www.sciencedirect.com/science/article/pii/S092479631300211X, 2014.

Skogen, M. D., Hjøllo, S. S., Sandø, A. B., and Tjiputra, J.: Future ecosystem changes in the Northeast Atlantic: a comparison between a global and a regional model system, ICES Journal of Marine Science, 75, 2355–2369, https://doi.org/10.1093/icesjms/fsy088, https://doi.org/10.1093/icesjms/fsy088, 2018.

Somavilla, R., Schauer, U., and Budéus, G.: Increasing amount of Arctic Ocean deep waters in the Greenland Sea, Geophysical Research Letters, 40, 4361–4366, https://doi.org/10.1002/grl.50775, https://agupubs.onlinelibrary.wiley.com/doi/abs/10.1002/grl.50775, 2013.

Stöven, T., Tanhua, T., Hoppema, M., and von Appen, W.-J.: Transient tracer distributions in the Fram Strait in 2012 and inferred anthropogenic carbon content and transport, Ocean Science, 12, 319–333, https://doi.org/10.5194/os-12-319-2016, https://os.copernicus.org/articles/12/319/2016/, 2016.

Takahashi, T., Olafsson, J., Goddard, J. G., Chipman, D. W., and Sutherland, S. C.: Seasonal variation of CO_2 and nutrients in the high-latitude surface oceans: A comparative study, Global Biogeochemical Cycles, 7, 843–878, https://doi.org/10.1029/93GB02263, https://agupubs.onlinelibrary.wiley.com/doi/abs/10.1029/93GB02263, 1993.

Tanhua, Toste; Hoppema, M.: Dissolved Inorganic Carbon (DIC), Total Alkalinity, Oxygen and other Hydrographic and Chemical Data Obtained During the R/V Polarstern Cruise ARKXXVII/1 (EXPOCODE 06AQ20120614) along the CLIVAR Repeat Section 75N in the North Atlantic Ocean from 2012-06-14 to 2012-07-15 (NCEI Accession 0162432). NOAA National Centers for Environmental Information., dataset, 2017.

Taylor, K. E., Stouffer, R. J., and Meehl, G. A.: An Overview of CMIP5 and the Experiment Design, Bulletin of the American Meteorological Society, 93, 485–498, https://doi.org/10.1175/BAMS-D-11-00094.1, https://doi.org/10.1175/BAMS-D-11-00094.1, 2012.

Terhaar, J., Kwiatkowski, L., and Bopp, L.: Emergent constraint on Arctic Ocean acidification in the twenty-first century, Nature, 582, 379–383, https://doi.org/10.1038/s41586-020-2360-3, https://doi.org/10.1038/s41586-020-2360-3, 2020a.

Terhaar, J., Tanhua, T., Stöven, T., Orr, J. C., and Bopp, L.: Evaluation of Data-Based Estimates of Anthropogenic Carbon in the Arctic Ocean, Journal of Geophysical Research: Oceans, 125, e2020JC016 124, https://doi.org/https://doi.org/10.1029/2020JC016124, https://agupubs.onlinelibrary.wiley.com/doi/abs/10.1029/2020JC016124, e2020JC016124 10.1029/2020JC016124, 2020b.

Tjiputra, J. F., Assmann, K., and Heinze, C.: Anthropogenic carbon dynamics in the changing ocean, Ocean Science, 6, 605–614, https://doi.org/10.5194/os-6-605-2010, https://os.copernicus.org/articles/6/605/2010/, 2010.

Tjiputra, J. F., Roelandt, C., Bentsen, M., Lawrence, D. M., Lorentzen, T., Schwinger, J., Seland, Ø., and Heinze, C.: Evaluation of the carbon cycle components in the Norwegian Earth System Model (NorESM), Geoscientific Model Development, 6, 301–325, https://doi.org/10.5194/gmd-6-301-2013, https://gmd.copernicus.org/articles/6/301/2013/, 2013.

Tjiputra, J. F., Grini, A., and Lee, H.: Impact of idealized future stratospheric aerosol injection on the large-scale ocean and land carbon cycles, Journal of Geophysical Research: Biogeosciences, 121, 2–27, https://doi.org/https://doi.org/10.1002/2015JG003045, https://agupubs.onlinelibrary.wiley.com/doi/abs/10.1002/2015JG003045, 2016.

Turley, C. M., Roberts, J. M., and Guinotte, J. M.: Corals in deep-water: will the unseen hand of ocean acidification destroy cold-water ecosystems?, Coral Reefs, 26, 445–448, https://doi.org/10.1007/s00338-007-0247-5, https://doi.org/10.1007/s00338-007-0247-5, 2007.

Uppström, L. R.: The boron/chlorinity ratio of deep-sea water from the Pacific Ocean, Deep Sea Research and Oceanographic Abstracts, 21, 161 – 162, https://doi.org/https://doi.org/10.1016/0011-7471(74)90074-6, http://www.sciencedirect.com/science/article/pii/0011747174900746, 1974.

van Heuven, S., Pierrot, D., Rae, J., Lewis, E., and Wallace, D.: MATLAB Program Developed for CO_2 System Calculations, ORNL/CDIAC-105b. Carbon Dioxide Information Analysis Center, Oak Ridge National Laboratory, US Department of Energy, Oak Ridge, Tennessee., 2011.

van Vuuren, D. P., Edmonds, J., Kainuma, M., Riahi, K., Thomson, A., Hibbard, K., Hurtt, G. C., Kram, T., Krey, V., Lamarque, J.-F., Masui, T., Meinshausen, M., Nakicenovic, N., Smith, S. J., and Rose, S. K.: The representative concentration pathways: an overview, Climatic Change, 109, 5, https://doi.org/10.1007/s10584-011-0148-z, https://doi.org/10.1007/s10584-011-0148-z, 2011a.

van Vuuren, D. P., Stehfest, E., den Elzen, M. G. J., Kram, T., van Vliet, J., Deetman, S., Isaac, M., Klein Goldewijk, K., Hof, A., Mendoza Beltran, A., Oostenrijk, R., and van Ruijven, B.: RCP2.6: exploring the possibility to keep global mean temperature increase below 2°C, Climatic Change, 109, 95, https://doi.org/10.1007/s10584-011-0152-3, https://doi.org/10.1007/s10584-011-0152-3, 2011b.

Våge, K., Pickart, R. S., Spall, M. A., Moore, G., Valdimarsson, H., Torres, D. J., Erofeeva, S. Y., and Nilsen, J. E. Ø.: Revised circulation scheme north of the Denmark Strait, Deep Sea Research Part I: Oceanographic Research Papers, 79, 20 – 39, https://doi.org/https://doi.org/10.1016/j.dsr.2013.05.007, http://www.sciencedirect.com/science/article/pii/S0967063713001040, 2013.

Våge, K., Moore, G., Jónsson, S., and Valdimarsson, H.: Water mass transformation in the Iceland Sea, Deep Sea Research Part I: Oceanographic Research Papers, 101, 98 – 109, https://doi.org/https://doi.org/10.1016/j.dsr.2015.04.001, http://www.sciencedirect.com/science/article/pii/S0967063715000680, 2015.

Wallace, D. W. R. and Deming, J.: Dissolved inorganic carbon, alkalinity, temperature, salinity and other variables collected from discrete sample and profile observations using CTD, bottle and other instruments from the USCGC POLAR SEA in the North Greenland Sea from 1992-07-15 to 1992-08-14 (NCEI Accession 0115687). NOAA National Centers for Environmental Information., https://doi.org/10.3334/cdiac/otg.carina$_3$2l919920715, $dataset$, 2014.

Wu, Y., Hain, M. P., Humphreys, M. P., Hartman, S., and Tyrrell, T.: What drives the latitudinal gradient in open-ocean surface dissolved inorganic carbon concentration?, Biogeosciences, 16, 2661–2681, https://doi.org/10.5194/bg-16-2661-2019, https://bg.copernicus.org/articles/16/2661/2019/, 2019.

Yukimoto, S., Yoshimura, H., and Hosaka, M.: Meteorological Research Institute-Earth System Model v1 (MRI-ESM1)—Model Description.Technical Report of MRI. Ibaraki, Japan, 88 pp., Tech. rep., 2011.

Zeebe, R. and Wolf-Gladrow, D.: CO_2 in Seawater: Equilibrium, Kinetics, Isotopes, vol. 65 of *Elsevier Oceanography Series*, Elsevier Science, 1 edn., 2001.

Zheng, M.-D. and Cao, L.: Simulation of global ocean acidification and chemical habitats of shallow- and cold-water coral reefs, Advances in Climate Change Research, 5, 189–196, https://doi.org/https://doi.org/10.1016/j.accre.2015.05.002, https://www.sciencedirect.com/science/article/pii/S1674927815000210, including special topic on China's carbon emissions peaking, 2014.